ADVANCED HEALTHCARE MATERIALS
www.advhealthmat.de

Emerging Applications of Photodynamic and Sonodynamic Therapies in Orthopedic Disorders: Mechanisms, Challenges, and Future Directions

Peiyang Wen, Wenqing Xie, Da Zhong, Zhou Li,* and Yusheng Li**

As non-invasive targeted therapeutic modalities, photodynamic therapy (PDT) and sonodynamic therapy (SDT) have demonstrated significant clinical potential in orthopedic disorders management. PDT generates reactive oxygen species (ROS) through photosensitizer activation under specific light wavelengths, selectively inducing apoptosis in pathological cells. SDT employs sonosensitizers activated by low-intensity ultrasound to produce ROS while offering enhanced depth of tissue penetration. Current advancements reveal clinical efficacy in bone tumor ablation, management of osteomyelitic infections, intervention for degenerative bone diseases, and bone regeneration applications. However, clinical translation faces three principal challenges: i) PDT's photonic penetration constraints coupled with tumor tissue hypoxia; ii) SDT efficacy limitations from inhomogeneous energy dispersion in therapeutic acoustic fields and challenges in precise modulation of inertial cavitation thresholds; iii) Persistent standardization deficits in longitudinal biosafety assessment frameworks and treatment dosimetry. This review systematically elucidates molecular mechanisms and targeted regulatory pathways of PDT/SDT for orthopedic pathologies, critically evaluates therapeutic efficacy based on preclinical and clinical evidence, and proposes translational strategies focusing on novel sensitizer development, combination therapeutic strategies, and intelligent platform technologies. Future investigations should prioritize sensitizer structural optimization, establishment of standardized treatment protocols, and integration of multimodal image-guided systems to facilitate comprehensive clinical translation of PDT/SDT in precision orthopedics.

1. Introduction

Orthopedics, a major subspecialty of surgery, is dedicated to the diagnosis and management of injuries and disorders affecting the musculoskeletal system, including osseous structures (bones), skeletal muscles, tendons, ligaments, cartilage and other soft tissues, as well as major articulations such as knees, ankles, spinal joints, hand-foot complexes, and shoulder-elbow regions.[1] This discipline encompasses multiple subspecializations including trauma and fracture management, musculoskeletal infections, orthopedic oncology, sports medicine, deformity correction, and arthroplasty (joint replacement). Pathological conditions of the musculoskeletal system—such as infections, traumatic injuries, and neoplastic lesions—can induce structural damage to bones, cartilage, muscles, tendons, or ligaments, ultimately resulting in musculoskeletal disorders (MSDs). Recent data show ≈1.3 billion people globally suffer from MSDs. Prevalence is projected to escalate with population aging, imposing a substantial healthcare burden.[2,3]

Therapeutic strategies for MSDs are broadly classified into two primary modalities: operative intervention and nonoperative management, both of which are indispensable components in

P. Wen, W. Xie, D. Zhong, Y. Li
Deparment of Orthopedics
Xiangya Hospital
Central South University
Changsha, Hunan 410008, China
E-mail: zhongda@csu.edu.cn; liyusheng@csu.edu.cn
P. Wen
Xiangya School of Medicine
Central South University
Changsha, Hunan 410083, China
W. Xie, D. Zhong, Y. Li
National Clinical Research Center for Geriatric Disorders
Xiangya Hospital
Central South University
Changsha, Hunan 410008, China
Z. Li
Tsinghua Changgung Hospital
School of Clinical Medicine
Tsinghua University
Beijing 100084, China
E-mail: li_zhou@tsinghua.edu.cn
Z. Li
School of Biomedical Engineering
Tsinghua University
Beijing 100084, China

The ORCID identification number(s) for the author(s) of this article can be found under https://doi.org/10.1002/adhm.202502565

DOI: 10.1002/adhm.202502565

contemporary MSD treatment paradigms.[4] In cases of severe osseous pathology with extensive tissue compromise, surgical procedures paired with chemotherapeutic regimens remain unavoidable. However, conventional surgical approaches exhibit limited therapeutic efficacy and inherent invasiveness, while traditional chemotherapeutic agents carry risks of systemic toxicity and off-target adverse effects.[2] Recent advancements in precision medicine have propelled nonoperative therapeutic strategies to the forefront of musculoskeletal disease management, now recognized as pivotal determinants in achieving successful clinical outcomes.[5] Structurally tunable nanodrug delivery systems (NDDS) have emerged as focal materials in nonsurgical therapeutics, achieving pathological organ targeting via directional functionalization of chemical moieties, while enabling exogenous stimulation-actuated on-demand payload release to precisely trigger aberrant cellular apoptosis.[6] Nevertheless, such systems still fundamentally rely on conventional cytotoxic chemotherapeutics, thus failing to resolve the intrinsic toxicity limitations of systemic chemotherapy. Emerging PDT and SDT modalities present innovative solutions that circumvent both the invasiveness of surgical procedures and the nonspecific toxicity profiles associated with chemotherapeutic interventions in orthopedic oncology.

Photodynamic therapy (PDT) and sonodynamic therapy (SDT) have garnered multidisciplinary research attention as targeted, remotely controllable, and non-invasive therapeutic techniques, owing to their spatiotemporally precise control characteristics.[7,8] The conceptual origin of PDT can be traced to 1900, when researchers first observed acridine dye-induced cytotoxicity under light exposure,[9] a landmark discovery that established the theoretical foundation for photosensitizer-mediated targeted therapy. With technological progression, SDT emerged as a derivative strategy of PDT, utilizing ultrasound activation instead of light to overcome tissue penetrability limitations. Both modalities have achieved significant clinical success in managing superficial tissue pathologies, particularly breast and skin cancers. This trajectory originated with T. J. Dougherty's landmark 1979 application of hematoporphyrin derivative (HPD) in PDT for breast cancer,[10] sparking ongoing advancements in sensitizer development. Representative breakthroughs include the Fe_3O_4@ZnO-Bru nanosystem by Ren's team,[11] which achieves combined PDT/CDT for cutaneous squamous carcinoma, and Wang et al.'s IR780@PLGA@HM composite microparticles,[12] demonstrating effective suppression of breast cancer bone metastasis through SDT-immunomodulation synergy. Despite the demonstrated efficacy of PDT and SDT in oncology and superficial tissue diseases, their translational application in MSD remains notably delayed. This gap primarily stems from two critical limitations: i) The unique anatomical architecture of the musculoskeletal system complicates energy propagation and sensitizer distribution; ii) The physical properties of highly mineralized bone matrices significantly reduce near-infrared light penetration efficiency, while rapid ultrasound attenuation in cortical bone restricts SDT effectiveness in deep-seated lesions.

In recent years, PDT and SDT have attracted growing research interest as emerging modalities for managing bone-related pathologies. Investigators have engineered multifunctional responsive nanomaterials and introduced novel therapeutic strategies (PDT/SDT-based modalities) to overcome limitations of conventional approaches in treating diverse skeletal disorders, including bone neoplasms, osteomyelitis, osteoarthritis, rheumatoid arthritis (RA), and compromised osseous regeneration. This review systematically outlines the fundamental mechanisms underlying PDT and SDT, examines recent advancements in photosensitizer and sonosensitizer design tailored for skeletal applications, and proposes potential translational pathways for optimizing these photonic and acoustic therapies in orthopedic clinical practice.

2. Fundamental Mechanisms of PDT and SDT

2.1. PDT Mechanisms: Type I/II Reactions, Oxygen Dependency, and Nanosensitizer Design

PDT is a specialized non-surgical treatment that delivers photosensitizers (PS) to target lesions. Under aerobic conditions, PS is activated by light of specific wavelengths and energy, generating reactive oxygen species (ROS) to induce apoptosis of abnormal cells at the lesion site.[13,14] Upon systemic administration, PS initiates photodynamic reactions through two distinct, ROS-dependent mechanisms, as illustrated in **Figure 1A**. Both mechanisms share an identical initial phase: ground-state PS (S_n) absorbs photons to reach an excited singlet state (S_1) and partially releases energy through fluorescence, with residual energy driving intersystem crossing to form a triplet excited state (T_1-PS).[15,16] Subsequently, T_1-PS proceeds through divergent pathways:

In the first mechanism (Type I reaction), T_1-PS transfers hydrogen atoms or electrons to nearby biomolecules, generating free radicals—primarily superoxide anion ($O_2\cdot^-$), which initiates intracellular ROS propagation. This triggers an oxidative cascade, resulting in massive ROS accumulation that damages pathological cells at the lesion site.[15–17] Conversely, the second mechanism (Type II reaction) involves direct energy transfer from T_1-PS to triplet ground-state oxygen ($^3O_2$) dissolved in extracellular spaces, forming highly reactive singlet oxygen ($^1O_2$) without PS decomposition or direct cellular structural damage.[15,16]

Although Type II reactions are generally dominant in PDT efficacy, the relative contributions of these mechanisms depend on multiple factors including oxygen concentration, pH levels, structural properties of PS, and tissue-specific characteristics of lesions.[18] Notably, Type I reactions prevail under hypoxic conditions when extracellular oxygen reserves are depleted.

Critical to PDT success, PS directly determines therapeutic outcomes. Clinically available PS agents encompass porphyrins (hematoporphyrin, Photofrin, protoporphyrin IX), porphyrin derivatives (5-aminolevulinic acid, benzoporphyrin derivatives, chlorins), photosensitive dyes (acridine orange, methylene blue, indocyanine green), as well as metallic and semiconductor nanoparticles.[14,16] The relevant information regarding photosensitizers has been consolidated and systematically summarized in **Table 1**.

2.2. SDT Mechanisms: Inertial Cavitation, Pyrolytic ROS, and Dynamic Drug Release

Light therapy has been utilized as a non-invasive treatment across multiple clinical specialties for decades, yet it faces inherent lim-

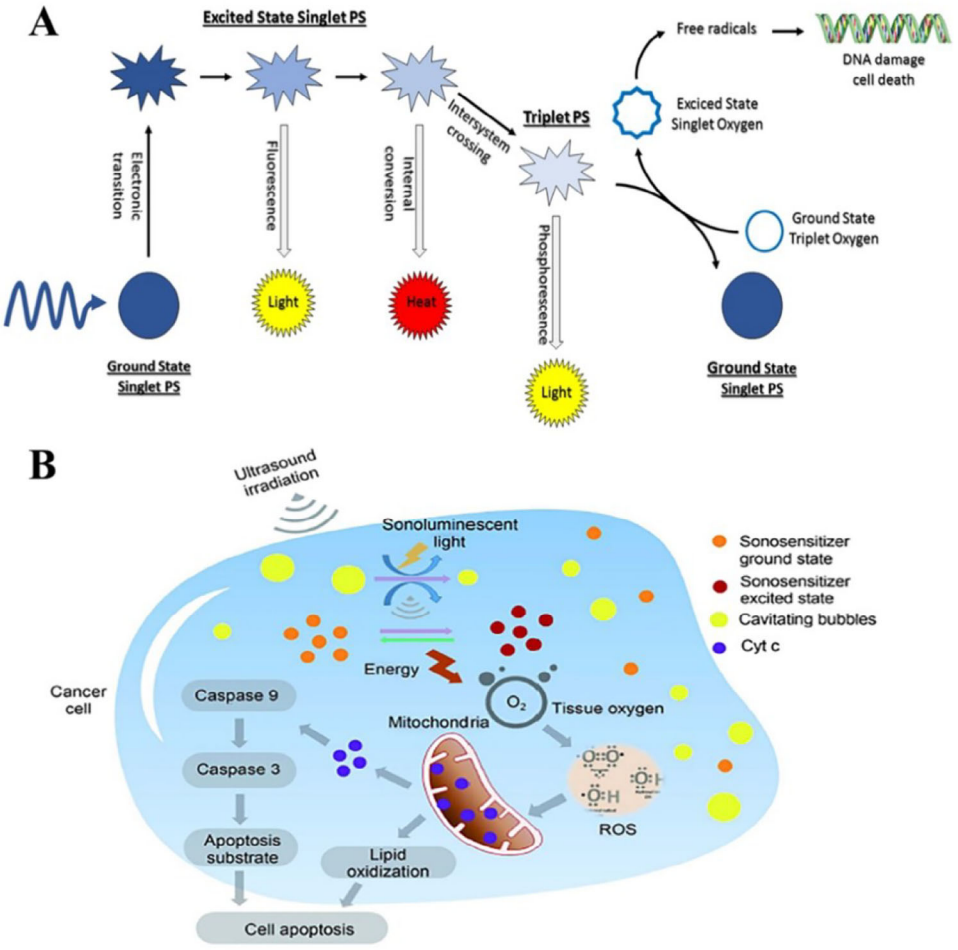

Figure 1. PDT versus SDT: ROS generation mechanisms. A) Mechanistic diagram of the photodynamic reaction. Reproduced with permission.[16] Copyright 2018, Elsevier. B) Schematic illustration of SDT. Reproduced with permission.[22] Copyright 2020, Royal Society of Chemistry (RSC).

itations: i) limited light penetration depth restricts its efficacy in treating deep-seated lesions, as light activation remains mandatory for photosensitizers; ii) post-PDT nanoparticle retention in tissues may induce adverse effects.[19] SDT, combining low-intensity US with sono-sensitizing agents, overcomes these constraints by enabling energy delivery to light-inaccessible deep organs, notably the liver and pancreas. Analogous to PDT, SDT generates substantial ROS through interactions among US, sonosensitizers, and tissue oxygen under non-toxic conditions involving both US and sensitizing agents.

While PDT mechanisms are well-characterized, SDT's mechanistic underpinnings remain incompletely understood. Proposed mechanisms include sonoluminescence, pyrolysis, ROS generation via cavitation-induced bubble collapse, and ROS-independent cytotoxicity.[20] US interaction with aqueous environments induces cavitation—classified into stable and inertial types. Stable cavitation involves oscillatory bubble motion around equilibrium radii through multiple acoustic compression–decompression cycles, generating shear forces for fluid mixing. Conversely, inertial cavitation involves rapid bubble expansion followed by violent collapse under US, producing extreme localized conditions (≤10 000 K, 81 MPa) that activate cell-bound sonosensitizers. Energy released during sensitizer relaxation excites ambient molecular oxygen, generating ROS with indirect cytotoxic effects.[21] The possible mechanisms of SDT are summarized in Figure 1B.

Building upon these two cavitation modalities, research teams led by Son and Kim proposed two fundamental mechanisms to elucidate ROS generation in SDT.[22] The first mechanism, termed sonoluminescence, involves light emission during ultrasound irradiation of aqueous solutions. While the underlying origin remains elusive, this phenomenon may originate from blackbody radiation, bremsstrahlung, or recombination radiation mechanisms. The emitted light activates sonosensitizers, inducing ROS production through processes analogous to PDT. The second mechanism, pyrolysis, utilizes extreme temperatures produced by inertial cavitation to fragment sonosensitizers. This initiates aqueous pyrolysis, yielding hydroxyl radicals (·OH) that react with endogenous substrates to generate cytotoxic ROS.

Sonosensitizers critically determine SDT efficacy, serving as its core therapeutic component (**Table 2**). Since the advent of SDT, a broad spectrum of sensitizers has been engineered, encompassing organic molecules, inorganic nanoparticles, and metal-organic frameworks.Early SDT research primarily adapted photosensitizers validated in PDT, such as porphyrins and cyanines, which generate ROS-dependent cytotoxicity under US excitation.

Table 1. Photodynamic therapy-based nanoparticles.

Application	Sensitizer	Conjugation	Cells/bacteria	Animal species	Research stages	Laser	Outcome	Ref
OS	PpIX	N/P@MCC	U2OS cells	OS mice	In vitro, in vivo	630 nm, 150 mW cm^{-2} OR 980 nm, 1 W cm^{-2}	PDT/PTT; IRT and FL imaging	[30]
	TPPS	TPPS@FNPs-MSC	U2OS cells	OS mouse	In vitro, in vivo	405 nm, 0.16 J s^{-1}	PDT/CDT; superior biocompatibility, high specificity for OS targeting	[37]
	TAPP	SPN-TAPP-PCB4	–	OS mice	In vitro, in vivo	650 nm, 0.5 W cm^{-2}	PDT/CDT; hypoxia-responsive nanomedicine for overcoming the hypoxic TME	[38]
	Ce6	Ce6@PPC-aCD47	K7M2 cells	OS mice	In vitro	660 nm, 1 W cm^{-2}	PDT and ICD; dual pH-sensitive nanodrug	[41]
	Ce6	A-NPs@(SHK+Ce6)	K7M2, Raw264.7, and L929 cells	OS mice	In vitro, in vivo	650 nm, 300 mW cm^{-2}	PDT and ICD; coregulate the acidic TME and TAM polarization to reprogram the TIME; High specificity for OS targeting	[42]
	Ce6	Ce6@SRF@RDV	MG63 and 143B cells	OS mice	In vitro, in vivo	660 nm	Red blood cell-derived vehicle; Safety compared with traditional PDT and ferroptosis therapy	[44]
	Ce6	MPCT@Li-R	MNNG/HOS cells	OS mice	In vitro, in vivo	660 nm, 500 mW cm^{-2}	Pt NPs promote the production of ROS during PDT; MTH1 inhibitors amplify the therapeutic effect of oxidative damage	[45]
	MB	HA-NPs-MB	Saos-2 cells	OS mice	In vitro, in vivo	808 nm, 50 mW cm^{-2}	Better efficiency of PDT; less MB be used	[56]
	ICG	PEG-GO-FA/ICG-Rg3	MG63 and U2OS cells	OS mice	In vitro, in vivo	808 nm	Ginsenoside Rg3; NPs improve PDT in inhibiting malignant progression and stemness of osteosarcoma cell	[57]
	ICG	TPP-PPG@ICG	MG63 cells	OS mice	In vitro, in vivo	808 nm, 0.6 W cm^{-2}	Mitochondria-targeting PDT; Fluorescence imaging-guided synergistic phototherapy	[58]
	AlPcS4	AlPcS4@FNPs	MG63, Saos 2 and U2OS cells	OS mice	In vitro, in vivo	405 nm	MSC enhance the effectiveness of PDT	[60]
	ZnPc	PEG-PMAN/ZnPc	MNNG/HOS cells	OS mice	In vitro, in vivo	660 nm, 1.8 kJ cm^{-2}	Mitochondrial-targeting specificity; Superior PDT efficacy; High biocompatibility	[61]
	BODIPYs	H-MnSiO2/KB-ALD	HOS cells	OS mice	In vitro, in vivo	808 nm, 0.5 W cm^{-2}	Attenuate circadian rhythm amplitude in OS cells; Overcome hypoxic TME	[63]
	IR780	D@SLNP@OSM-IR780	K7M2 cells	OS mice	In vitro, in vivo	808 nm, 2 W cm^{-2}	PDT/CDT; Mitochondrial-targeting specificity	[64]
	–	RhRu/Ti3C2Tx	143B cells	OS mice	In vitro, in vivo	808 nm, 0.56 W cm^{-2}	PDT/PTT/CDT	[67]
	MXene	CeO_2@MXene	143B cells	OS mice	In vitro, in vivo	808 nm, 1 W cm^{-2}	Overcome hypoxic TME; Combine I and II type PDT	[69]
	–	Pd@Pt-PEG	LM8 and L929 cells	OS mice	In vitro, in vivo	808 nm, 1 W cm^{-2}	PDT/PTT; Overcome hypoxic TME; FL/PT imaging-guided synergistic PTT/PDT treatment	[70]
	AgBiS2	AgBiS2 NPs	UMR-106 cells	OS mice	In vitro, in vivo	808 nm, 1 W cm^{-2}	PDT/PTT; Antibacterial activity and CT imaging	[71]
	CP	CP-SiNPs	U2OS cells	–	In vitro	350 nm, 0.27 mW cm^{-2}	CP-loaded silica nanoparticles boosted photodynamic therapy through enhanced bioavailability	[79]
Osteomyelitis	PpIX	Van-GQDs/PpIX	*Escherichia coli*	–	In vitro	X-ray (2 Gy, 6 MV)	PDT/CDT; Destroys cell walls; combats deep-seated infections	[101]

(*Continued*)

Table 1. (Continued)

Application	Sensitizer	Conjugation	Cells/bacteria	Animal species	Research stages	Laser	Outcome	Ref
	LD40	–	*S. aureus* (MRSA)	Osteomyelitis rat	In vitro, in vivo	650 nm, 25 J cm^{-2}	PACT; Enhances bone matrix regeneration and effectively eradicates drug-resistant bacteria in deep bone infections	[102]
	ICG	BMUIG	*S. aureus*	Osteomyelitis mouse	In vitro, in vivo	808 nm, 0.1 W cm^{-2}	PACT; Dual-modality imaging (photoacoustic/MRI); Synergistic high-efficacy antibacterial action at low doses	[105]
IAIs	ICG	Ti-M/I/RGD	*S. aureus*	IAIs rat	In vitro, in vivo	808 nm, 1 W cm^{-2}	PDT/PTT; Biofilm eradication; High-efficacy anti-IAIs	[106]
	Ce6	BSA@MnO2 @Ce6@Van, BMCV	*S. aureus* (MRSA)	IAIs mice	In vitro, in vivo	660 nm	PACT and ICD; Biofilm eradication; Establish long-term immune memory	[107]
Osteomyelitis	AD-Ce6/Apt	AA-MAR	*S. aureus*	Osteomyelitis rat	In vitro, in vivo	660 nm, 0.6 W cm^{-2}	Spatiotemporally programmed regulation of immune microenvironment; PDT-driven synergy: antibacterial activity, immunomodulation, and bone remodeling	[108]
	–	BP/BQD	*S. aureus*	Osteomyelitis mice	In vitro, in vivo	–	Phosphorescence replaces conventional laser to enable dynamic phosphorescence-ROS conversion	[110]
IAIs	–	Cu_9S_8 NPs	*S. aureus*	–	In vitro	808 nm, 1 W cm^{-2}	PDT/PTT; Biofilm eradication	[113]
RA	HYP	HYP-EMLs	–	AIA rat	In vivo	590 nm	Integration of EMLs, Ho-MNs, and PDT-driven light-controlled release enables deep drug penetration with precise spatiotemporal regulation	[127]
	5-ALA	5-ALA@DMNA	RA-FLS/FLS	CIA rat	In vitro, in vivo	635 nm, 100 mW cm^{-2}	PDT and immunoregulation; Overcome the skin barrier to achieve localized and efficient delivery	[128]
	TSPP	TP	FLS	CIA rat	In vitro, in vivo	500–550 nm	PDT/bio-imaging; Modulate the inflammatory microenvironment and reduce IL-17 and TNF-α levels	[130]
	IR780	Au-DEN-MTX-IR780 NPs	Macrophage (RAW264.7)	–	In vitro	808 nm, 0.5 W cm^{-2}	PDT/PTT/CDT; Dual-targeting effect	[132]
	CuS	Au NR@CuS	FLS	CIA rat	In vitro, in vivo	808 nm, 0.5 W cm^{-2}	PDT/PTT/CDT; Suppression of synovitis cell activity; Efficient inhibition of synovial hyperplasia; High drug-loading capacity	[135]
	–	FT-HA-MTX NPs	Macrophage (RAW264.7)	AIA rat	In vitro, in vivo	660 nm, 1 W cm^{-2}	PDT/PTT/CDT; HA-mediated targeted delivery; Significantly reduced levels of pro-inflammatory cytokines TNF-α and IL-1β	[136]
	–	T-PS	–	CIA mice	In vivo	665 nm, 50 mW cm^{-2}	PDT; precision imaging; Induces apoptosis, vascular damage, and local hemorrhage within lesioned joints without photodamage-related side effects	[138]

(*Continued*)

Table 1. (Continued)

Application	Sensitizer	Conjugation	Cells/bacteria	Animal species	Research stages	Laser	Outcome	Ref
	BiNS	siBiMPNH	FIS	CIA rat	In vitro, in vivo	808 nm 1 W cm^{-2} OR 660 nm 0.5 W cm^{-2}	PDT/PTT; Immune modulation and synovial microenvironment remodeling	[141]
HO	IR-808	WL-808	Chondrocytes	HO mice	In vitro, in vivo	808 nm, 1 W cm^{-2}	PDT induces chondrocyte apoptosis for HO treatment; Type II collagen serves as a key therapeutic target in HO	[150]
Bone fracture	IR780	Ti-RP-IR780-RGDC	–	Rat	In vivo	808 nm, 0.5 W cm^{-2}	PDT/PTT; Enhance osseointegration and accelerate bone repair; Enable low-temperature sterilization to minimize tissue damage	[151]
Bone regeneration	TiO_{2-X}	KMNW and NaMNS	Osteoblasts (MC3T3-E1 ATCC CRL-2594)	Rabbit	In vitro, in vivo	808 nm, 0.7 W cm^{-2} or 1 W cm^{-2}	PDT/PTT; Effectively inhibit *S. aureus* and *E. coli*; Promote bone regeneration and osseointegration	[152]

However, their propensity for intracellular aggregation limited therapeutic efficacy. To address this limitation, nanotechnology-driven sonosensitizers were developed, where nanoparticle encapsulation enhances SDT efficiency through dual mechanisms: lowering cavitation energy thresholds and creating nucleation sites for microbubble formation. Recent advancements focus on metal oxide-based sonosensitizers (e.g., Fe_3O_4, tungsten oxides), which demonstrate synergistic US-responsive behavior. These materials enable ROS amplification via ultrasound-activated Fenton reactions, offering a dual-modal therapeutic strategy.[22,23]

2.3. Comparative Analysis: Similarities and Differences between PDT and SDT

PDT and SDT represent two distinct non-invasive modalities, both reliant on the synergistic interplay between sensitizers and exogenous energy (light or ultrasound) to generate ROS for targeted apoptosis induction in pathological cells. Therapeutic outcomes for both modalities hinge critically on sensitizer efficacy, with initial SDT protocols even adopting PDT-validated agents such as porphyrin derivatives due to their established ROS-generating properties.

PDT and SDT diverge mechanistically and clinically. PDT employs established ROS pathways: Type I generates free radicals via electron/hydrogen transfer, while Type II produces $^1O_2$ through direct energy transfer. SDT mechanisms remain incompletely resolved, potentially involving sonoluminescence, pyrolysis, or cavitation. Cavitation effects include stable oscillations that enhance mass transport and inertial collapses generating extreme conditions (>10 000 K, $\Delta P \approx 81$ MPa). Therapeutically, PDT's efficacy is limited by poor deep-tissue light penetration. SDT excels in treating internal targets via superior ultrasound penetration. PDT efficiency hinges on microenvironmental factors (oxygen, pH, sensitizer design), whereas SDT depends on cavitation control and sensitizer engineering—notably nanoencapsulation to lower cavitation thresholds.

Clinically, PDT presents biosafety concerns stemming from prolonged post-procedural photosensitizer retention, while SDT's therapeutic predictability is complicated by nonlinear ultrasound-biofluid interactions. Emerging synergies in sensitizer innovation are now evident, particularly with nano-engineered metal oxide platforms demonstrating dual-capacity ROS amplification and modality-specific limitation mitigation—features that strategically align with combinatorial therapeutic development paradigms.

3. Bone Tumors

Cancer has persisted as one of the most lethal diseases for centuries, consistently exhibiting high mortality rates worldwide. Bone tumors, which may originate intrinsically within bone tissues or arise from their constitutive components, pose significant clinical challenges. Both primary and metastatic bone tumors can severely compromise patients' quality of life.[24,25] Conventional surgical interventions provide only partial resolution while introducing associated complications such as functional impairment, often exacerbating patient morbidity. In contrast, PDT and SDT emerge as promising alternatives capable of circumventing these iatrogenic risks, thus representing advanced strategies for future bone tumor management.

3.1. PDT in Bone Tumors: Tumor-Specific Delivery and Hypoxia-Resistant Strategies

3.1.1. PDT with Porphyrins: Clinical Derivatives and ROS Amplification

Porphyrin-based compounds and their derivatives, including 5-aminolevulinic acid (5-ALA), hematoporphyrin monomethyl ether (HMME), protoporphyrin IX, and meta-tetra(hydroxyphenyl)chlorin (mTHPC), are commonly employed as photosensitizers. However, the standalone efficacy of these

Table 2. Sonodynamic therapy-based nanoparticles.

Application	Sensitizer	Conjugation	Cells/bacteria	Animal species	Research stages	Ultrasound	Outcome	Ref
OS	5-ALA	-	UMR-106 cells	OS mice	In vitro, in vivo	1.0 MHz, 2.0 W cm^{-2}	Suppresses the volume of implanted tumors in mice and the viability of UMR-106 cells; Targeting mitochondrial apoptosis	[87]
	IR780	MPIRx	K7M2 and 143B cells	OS mice	In vitro, in vivo	1.0 MHz, 1 W cm^{-2}	Remodeling the tumor immune microenvironment; Suppressing primary tumor growth along with pulmonary metastasis	[92]
Rhabdomyosarcoma	TiO_2	glu-aTiO_2/PEO-PPO	Rh30 cells	Mice	In vitro, in vivo	1.0 MHz, 1.2 W cm^{-2}	Precise control of nanoparticle surface functionalization; Glucose-mediated active targeting	[94]
OS	TiO_2	W-TiO_2	143B cells	OS mice	In vitro, in vivo	–	SDT/CDT; GSH depletion; Ultrasound tumor ablation; High biosafety	[95]
	FePCN	mFeP@si	143B and K7M2 cells	OS mice	In vitro, in vivo	1.0 MHz, 1 W cm^{-2}	siRNA-mediated gene silencing; Ferroptosis; Immunosuppressive TME remodeling; Overcoming chemotherapeutic resistance	[96]
OS/bone metastasis tumor	SP	$SPFeN_{OC}$	RAW264.7 and 4T1OS/ cells	Bone metastasis tumor mouse	In vitro, in vivo	–	SDT/CDT; Theranostics: NIR fluorescence/MR imaging; High-efficiency suppression of bone metastasis	[97]
Osteomyelitis	PpIX	HMMP	*S. aureus* and *E. coli*	Osteomyelitis mice	In vitro, in vivo	40 kHz, 1.5 W cm^{-2}	In situ vaccination; Immune activation and formation of immune memory	[114]
	g-ZnN_4	g-ZnN_4-MoS_2	*S. aureus* (MRSA)	Osteomyelitis rat	In vitro, in vivo	1.0 MHz, 1.5 W cm^{-2}	SDT; Highly efficient bactericidal activity and long-term osteoinductive capability; Superior long-term biocompatibility	[115]
	IR780	M2/IR780@PLGA	*S. aureus* (MRSA)	Osteomyelitis mice	In vitro, in vivo	1.0 MHz, 2 W cm^{-2}	SDT/Immunotherapy; M2 macrophages enable inflammation-targeted delivery; US and MR imaging	[116]
	CeTCPP	CeTCPP-Au	*S. aureus* and *E. coli*	Osteomyelitis rat	In vitro, in vivo	1.0 MHz, 2 W cm^{-2}	SDT and dynamic defect engineering; Enhanced ROS generation efficiency and deep-seated antibacterial therapeutic efficacy	[118]
	Porphyrinic MOF	D-PCN-2	*S. aureus* (MRSA)	Osteomyelitis rat	In vitro, in vivo	1.0 MHz, 1.5 W cm^{-2}	SDT; Defect engineering drives performance enhancement	[119]
	HNTM	RBC-HNTM-MoS_2	*S. aureus* (MRSA)	Osteomyelitis rat	In vitro, in vivo	1.0 MHz, 1.5 W cm^{-2}	Multimechanism synergistic antibacterial therapy: piezoelectric-enhanced sonocatalysis, US-driven mechanical force, and metabolic regulation achieve highly efficient bacterial eradication	[120]
	HNTM	RBC-HNTM-Pt@Au	*S. aureus* (MRSA)	Osteomyelitis rat	In vitro, in vivo	1.0 MHz, 1.5 W cm^{-2}	SDT-driven dynamic sterilization and toxin neutralization; Metal single-atom catalysts enhance sonocatalytic performance; Achieving a balance between high-efficiency antibacterial action and bone protection	[121]

(*Continued*)

Table 2. (Continued)

Application	Sensitizer	Conjugation	Cells/bacteria	Animal species	Research stages	Ultrasound	Outcome	Ref
	Au/TNT	Au/TNT@PG	*S. aureus* (MRSA)	Osteomyelitis rat	In vitro, in vivo	–	SDT combined with immunotherapy; Antibacterial-anti-inflammatory-osteogenic integrated design	[124]
RA	PpIX	Fe_3O_4-PPIX@Mφs	RAW264.7 macrophage cells	CIA mice	In vitro, in vivo	1.0 MHz, 2.0 W cm^{-2}	Synergistic triad of photosensitizer, nanocarrier, and bio-vehicle; Elimination of hyperplastic synovial cells and infiltrated inflammatory cells	[146]
	ICG	OI-NPs	FLS	–	In vitro	1.0 MHz, 1.0 W cm^{-2}	PSDT; ROS-mediated cytotoxicity; Amplify ROS generation capacity via oxygen-sensitizing strategy	[148]
	SPX	Rh/SPX-HSA	FLS	CIA mice	In vitro, in vivo	1.0 MHz, 1.0 W cm^{-2}	Dual functionality of inducing mitochondrial dysfunction and enzyme catalytic activity; Alleviation of the hypoxic microenvironment	[149]
Bone regeneration/osteomyelitis	HNTM	HN-Ti_3C_2	*S. aureus* (MRSA)/hBMSCs	Osteomyelitis rat	In vitro, in vivo	1.0 MHz, 1.5 W cm^{-2}	Highly effective antibacterial and anti-resistance properties; Sustained promotion of bone regeneration	[19]
	TiOx	CaO_2-TiOx@Ti_3C_2	*S. aureus*	Osteomyelitis mice	In vitro, in vivo	1.0 MHz, 1.0 W cm^{-2}	SDT/CDT; A chemical microenvironment integrating a sonosensitizer and self-supplied H_2O_2 was constructed; Ca^{2+} contributed to osteogenesis and repair functions	[157]
	MXene	VS_4/Mxene (VSM)	hBMSCs	SD rat	In vitro, in vivo	1.0 MHz, 1.2 W cm^{-2}	SDT/CDT; Ultrasound-induced sustained regulation of osteogenesis	[159]
	Mn/HSAE	Mn/HSAE@BCP	*S. aureus, E. coli* and hBMSCs	Osteomyelitis rabbit	In vitro, in vivo	2 W/cm^2	SDT/CDT; Combination of enzymatic catalysis and SDT; Integrating anti-infective, osteogenic, and high-biocompatibility properties	[160]

PS agents remains limited, driving extensive investigations into strategies such as nanoparticle-mediated PS delivery or targeted inhibition of specific signaling pathways to enhance their therapeutic performance.

As a PpIX precursor, 5-ALA is intracellularly metabolized and inhibits sarcoma cell proliferation at 100–200 μg mL^{-1}[26,27] while inducing apoptosis under blue light (436 nm).[28] Research indicates that receptor-interacting protein 3 (RIP3) exerts dual regulatory roles in 5-ALA-PDT: promoting apoptosis and autophagy while suppressing necrosis in U2OS osteosarcoma cells. Paradoxically, higher RIP3 levels correlated with improved U2OS cell survival post-treatment, highlighting RIP3 inhibition as a potential strategy to boost efficacy.[29] PpIX is seldom used independently; advancements focus on nanoparticle encapsulation. Chen et al. developed the biomimetic nanocarrier N/P@MCC, integrating nitrogen-doped graphene quantum dots (N-GQDs, exhibiting photothermal/PDT capabilities) and PpIX into catalase-functionalized hollow mesoporous nanospheres coated with cancer cell membranes. This system enhances PDT through catalase-mediated oxygen generation and synergistic ROS production (**Figure 2A**).[30] Similarly, silica nanoparticle-encapsulated PpIX (PpIX-SiNPs) outperformed free PpIX against osteosarcoma.[31]

Other derivatives show significant promise: HMME offers enhanced photodamage capacity and selectivity, exerting dose-/energy-dependent anti-proliferative effects in osteosarcoma models primarily via caspase pathway activation (Figure 2B).[32] While verteporfin (BPD-MA) induces tumor microvascular damage,[33] its clinical use is limited by side effects like photosensitivity.[10] Benzochloroporphyrin derivatives (BCPDs) overcome these with reduced photosensitivity, faster clearance, and improved penetration;[34] BCPD-17, for instance, effectively induces apoptosis/cell cycle arrest in Ewing's sarcoma (Figure 2C)[35] and reduces local recurrence rates post-osteosarcoma resection.[36]

Mesenchymal stem cell (MSC)-mediated delivery platforms, such as TPPS@FNPs-MSCs, exploit MSC tumor tropism to overcome distribution and internalization barriers. Irradiation effectively triggered ROS generation yielding potent anti-osteosarcoma activity (Figure 2D).[37] To counter PDT limi-

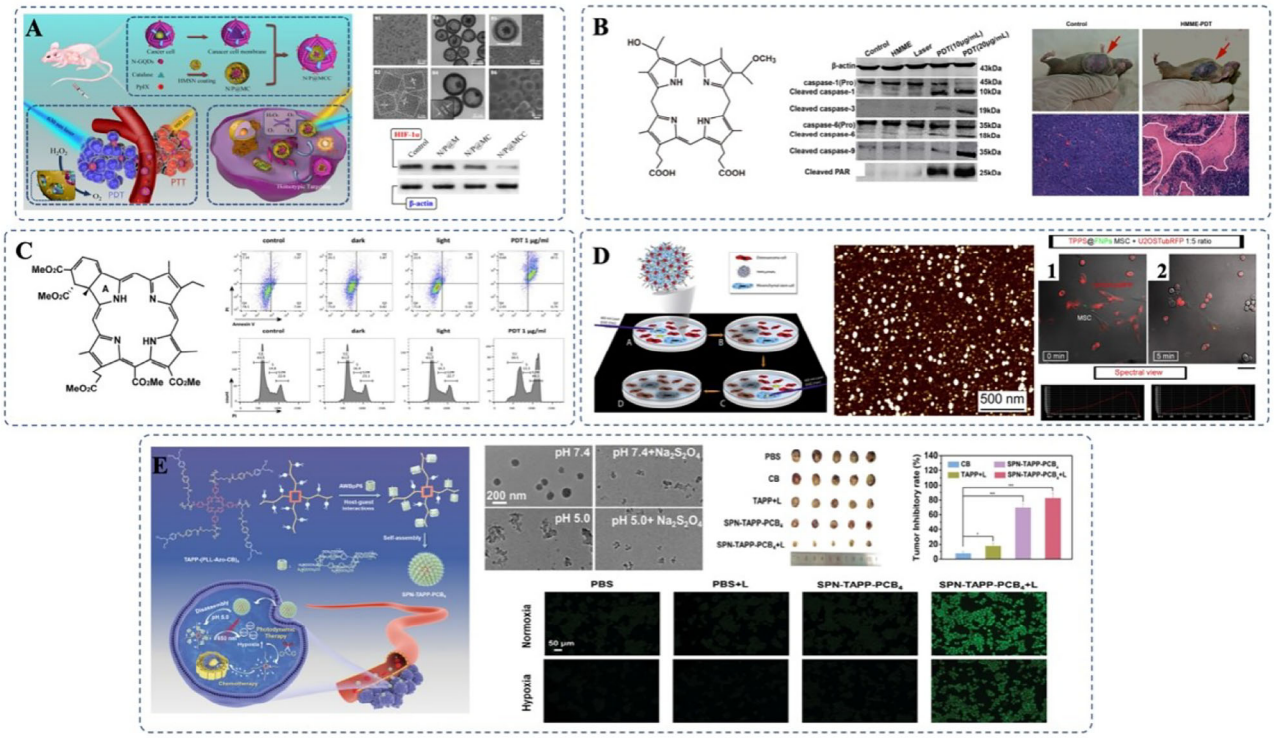

Figure 2. Hematoporphyrin-based PS in bone tumor applications. A) Homotypic-targeting bio-inspired catalytic nanocarrier N/P@MCC. Reproduced with permission.[30] Copyright 2021, American Chemical Society (ACS). B) Inhibitory effect of HMME-PDT on osteosarcoma cell proliferation via the caspase pathway. Reproduced with permission.[32] Copyright 2013, Public Library of Science. C) Molecular schematic and mechanistic effects of BCPDs. Reproduced with permission.[35] Copyright 2016, Elsevier. D) Porphyrin-loaded nanoparticle-integrated BMSC system TPPS@FNPs-BMSCs. Reproduced with permission.[37] Copyright 2013, Elsevier. E) Hypoxia-responsive tetrameric supramolecular peptide nanoprodrug SPN-TAPP-PCB4. Reproduced with permission.[38] Copyright 2023, Wiley-VCH.

tations posed by tumor hypoxia, Ding et al. engineered the hypoxia-responsive nanoprodrug SPN-TAPP-PCB4. Upon irradiation, the TAPP core generates ROS (primarily $^1O_2$), while the acidic/hypoxic tumor microenvironment triggers dissociation via azobenzene cleavage, releasing chlorambucil (CB) to combine PDT with hypoxia-activated chemotherapy (Figure 2E).[38] For the clinically prominent deep-penetrating PS mTHPC, liposomal encapsulation (Foslip) enhanced its potent anti-osteosarcoma effects (dose-dependent caspase activation/PARP cleavage) and metastasis suppression via optimized pharmacokinetics.[39,40]

3.1.2. Chlorophyll/Organic Dyes for PDT: Mitochondrial Targeting and Combination Therapy

Chlorin e6 (Ce6) is a widely used photosensitizer; however, its monotherapeutic application in PDT for bone tumors exhibits suboptimal efficacy. This limitation has spurred the development of nanoplatform-based Ce6 delivery systems to potentiate combination regimens or improve osteotropic targeting specificity.

To counter PDT limitations like metastasis and recurrence, Xiao et al.[41] engineered pH-dual-responsive polymeric nanovectors (Ce6@PPC-aCD47) via conjugation of an anti-CD47 antibody to Ce6-loaded micelles. The NPs can deliver anti-CD47 antibodies that enhance phagocytosis by TAMs/DCs and adaptive T-cell responses while Ce6-generated ROS induces direct cell death and immunogenic cell death (ICD) (**Figure** 3A). Similarly, Gao et al.[42] engineered an A-NPs@(SHK+Ce6) nanosystem that reprograms the immunosuppressive tumor microenvironment by shifting TAMs to the M1 phenotype via amplified ROS/ICD, enhancing CD8+ T-cell infiltration and reducing Tregs. Combined PD-1 blockade further achieved abscopal effects and immunological memory (Figure 3B).

Optimizing bone targeting is crucial. Li[43] addressed the low accumulation of freely administered Ce6/ZOL by developing Ce6@ZIF-PEG-ZOL nanoparticles, improving osteotropism and enabling dose-dependent apoptosis potentiation with 2-DG (Figure 3C). Concurrently, hemoglobin-rich erythrocyte-derived vesicles (Ce6@SRF@RDV) enable spatiotemporally precise co-delivery of Ce6 and sorafenib.[44] Laser-triggered membrane disruption facilitates tumor-localized release, permitting synergistic PDT and chemodynamic therapy (Figure 3D).

Tumor hypoxia and ROS detoxification (e.g., via MTH1 upregulation) constrain Ce6 efficacy. Song's platform MSN-Pt@Ce6/TH588@Liposome-RGD combats hypoxia with Pt NPs generating oxygen from H_2O_2 while Ce6 produces $^1O_2$. Acid-triggered release of the MTH1 inhibitor TH588 further amplifies oxidative stress by suppressing DNA repair (Figure 3E).[45] Deng et al. engineered an IrO_2@ZIF-8/BSA-FA(Ce6) nanocomposite that co-loads Ce6 onto hypoxia-relieving (catalase-mimetic) and photothermally active IrO_2 nanoparticles for targeted synergistic PDT/PTT (Figure 3F).[46]

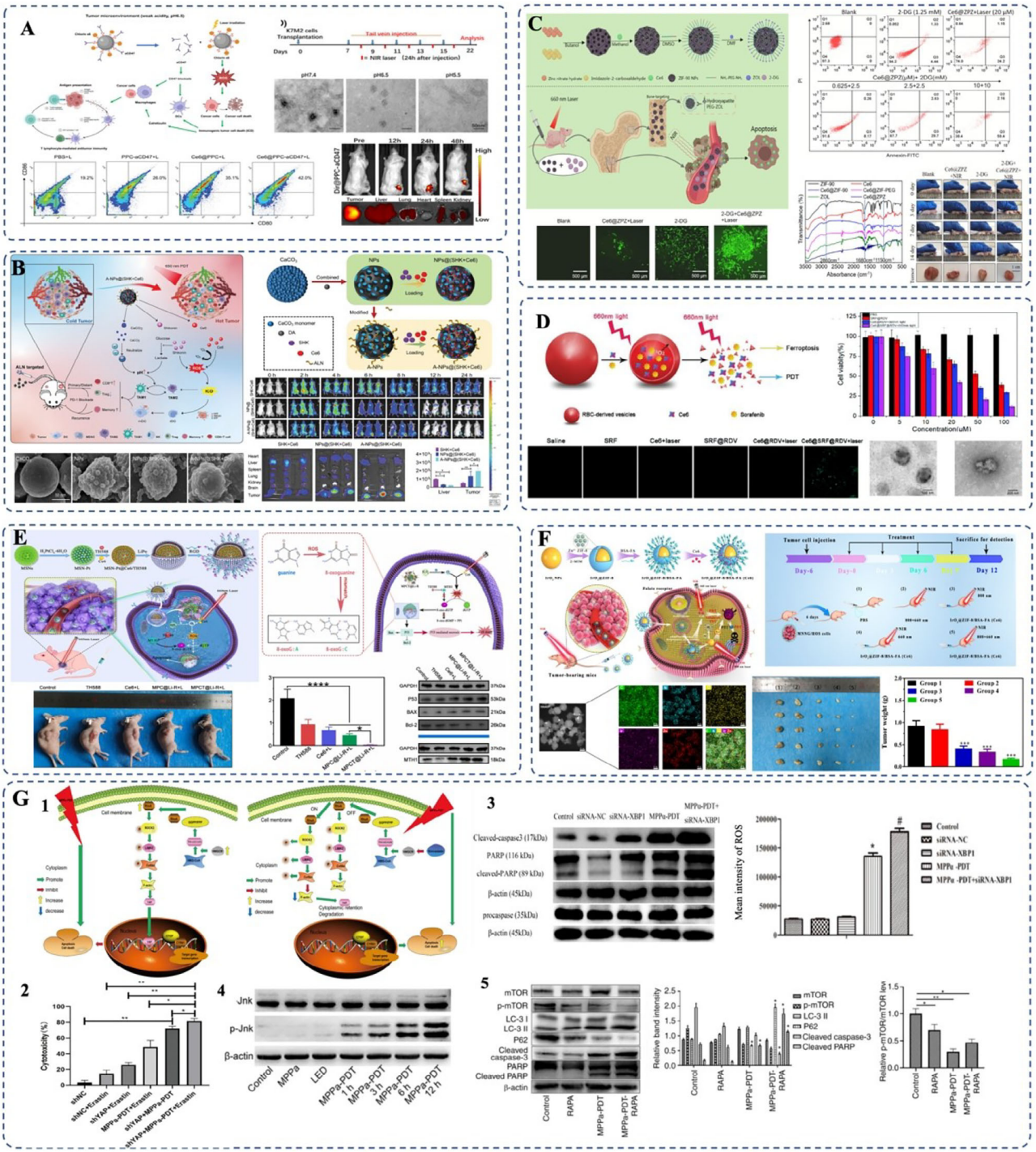

Figure 3. Chlorophyll-derived photosensitizers for osteosarcoma therapy. A) Dual pH-sensitive polymeric nanocarrier Ce6@PPC-aCD47. Reproduced with permission.[41] Copyright 2024, Tech Science Press. B) Calcium carbonate/polydopamine-based targeted nano-delivery system A-NPs@(SHK+Ce6). Reproduced with permission.[42] Copyright 2024, Wiley-VCH. C) Ce6@ZIF-PEG-ZOL with superior bone-targeting and high-efficiency drug delivery. Reproduced with permission.[43] Copyright 2024, Elsevier. D) PDT/CDT combinatorial strategy Ce6@SRF@RDV. Reproduced with permission.[44] Copyright 2021, Royal Society of Chemistry (RSC). E) MSN-Pt@Ce6/TH588@liposome-RGD (MPCT@Li-R) alleviating tumor hypoxia and ROS defense-mediated PDT resistance. Reproduced with permission.[45] Copyright 2022, Elsevier. F) Sodium iridium oxide (IrO_2) NPs with catalase-mimicking activity and photothermal effects. Reproduced with permission.[46] Copyright 2022, Taylor & Francis Online. G) MMPα-targeting photosensitizer. Reproduced with permission.[48,50–53] Copyright 2024, Impact Journals LLC.

The efficacy of pyropheophorbide-α (MMPα) against OS is hampered by intrinsic tumor cell resistance. Consequently, targeting molecular pathways to overcome MMPα-PDT resistance is crucial. Key regulators of ER stress, glucose-regulated protein 78 (GRP78) and protein kinase RNA-like endoplasmic reticulum kinase (PERK), are frequently overexpressed in malignancy. GRP78 knockdown sensitizes HOS cells to MMPα,[47] while combining MMPα-PDT with the PERK inhibitor GSK2656157 enhances OS cell apoptosis by suppressing autophagy and p21-mediated survival (Figure 3G1).[48] Conversely, activation of the RhoA/ROCK2/LIMK2/YAP axis promotes MMPα resistance in OS.[49] Dual suppression of YAP with ferroptosis inducers effectively restores MMPα susceptibility (Figure 3G-2).[50] Similarly, XBP1 silencing reduces antioxidant levels in HOS cells, suggesting potential synergy with MMPα-PDT (Figure 3G-3).[51] Mechanistically, MMPα induces MG-63 cell death primarily via mitochondrial apoptosis; however, it concurrently triggers compensatory autophagy through ROS-JNK signaling (Figure 3G-4).[52] Furthermore, MMPα-PDT inhibits AKT/mTOR proliferative signaling (Figure 3G-5), identifying mTOR as a potential target to enhance therapeutic outcomes.[53]

3.1.3. Dye Photosensitizers for PDT: Nanocarriers and Synergy Overcome Chemoresistance/Hypoxia

Acridine orange (AO) localizes subcellularly according to pH gradients. NIR irradiation activates lysosomal AO, generating ROS that disrupt lysosomes, inducing rapid OS cell death.[54] However, MDR cells retain AO predominantly in mitochondria, synergizing with doxorubicin to boost chemotherapeutic efficacy and circumvent resistance.[55] Hydroxyapatite nanoparticles (HA-NPs), osteocompatible due to structural mimicry of bone mineral, were conjugated with methylene blue (MB) to form HA-NPs-MB, enhancing PDT. This system protects MB from degradation, reduces required doses via controlled $^1O_2$ generation, and enables tumor-specific damage (**Figure 4A**).[56]

Despite superior biocompatibility, ICG exhibits limited clinical utility for bone tumors due to poor aqueous stability and rapid clearance. To overcome this, Lu et al.[57] developed PEG-GO-FA/ICG-Rg3 nanoparticles suppressing OS proliferation, tumor growth, and stemness under NIR (Figure 4B). Mitochondrial-targeted TPP-PPG@ICG impaired ATP production, reversing chemoresistance and inducing apoptosis[58] (Figure 4C). Additionally, Jiang et al.[59] engineered bone-affine ZIF-8 nanocarriers (ICG/Cyt c@ZZF-8) with surface modification for stability, enabling pH-triggered ROS generation and targeted ablation (Figure 4D).

Tetra-sulfonated aluminum phthalocyanine (AlPcS4) was loaded into fluorescent nanoparticles and functionalized onto MSCs, preserving MSC migration/viability for cell-mediated OS targeting and therapy, bypassing traditional carrier limitations.[60] Zinc phthalocyanine (ZnPc), despite superior attributes, is water-insoluble. Yu et al.[61] encapsulated ZnPc in an amphiphilic PEG-PMAN copolymer (PPZ), amplifying intracellular ROS, causing mitochondrial dysfunction (Figure 4E), and provoking G2/M cell cycle arrest and apoptosis in OS cells. Subsequent work demonstrated PPZ's synergy with tumor excision, highlighting its adjuvant potential.[62]

Ge et al.[63] co-encapsulated near-infrared BODIPY dyes and KL001 (a small-molecule inhibitor of cryptochrome (CRY)) within MnO_2 nanocapsules modified with alendronate (ALD), yielding the H-$MnSiO_2$/KB-ALD system. This formulation suppressed OS circadian rhythm amplitude, disrupted mitochondrial respiration via CRY inhibition, elevated intracellular oxygen to overcome hypoxia, and enhanced PDT efficacy (Figure 4F), pioneering circadian modulation for tumor PDT.

IR780, a heptamethine cyanine fluorophore with robust photodynamic properties, has been exploited for OS treatment. Zhang et al.[64] engineered IR780-modified osteosarcoma cell membrane (OSM)-camouflaged biomimetic lipid nanoparticles to achieve tumor homotypic targeting and mitochondria-directed drug delivery, establishing the D@SLNP@OSM-IR780 platform. Similarly, Wang et al.[65] developed PLGA-IR780 encapsulated in HOS cells (MH-PLGA-IR780), enhancing FL/PA imaging and triggering mitochondrial apoptosis/ferroptosis to improve PDT efficiency (Figure 4H), thereby advancing OS-targeted PDT.

3.1.4. Alternative PDT Strategies

Nano-Architectural Particles with Novel Metal-Element-Based Functional Groups: Conventional photosensitizers face limitations like poor solubility, instability, and low photosensitivity, driving development of metal-centric nanoparticles for PDT. Titanium dioxide (TiO_2) generates ROS under UV to kill cancer cells.[66] Beyond TiO_2, diverse metallic nanoparticles (Rh, Ru, Ce) have emerged. Liang et al.[67] synthesized bimetallic RhRu nanozymes on $Ti_3C_2T_x$ nanosheets (RhRu/$Ti_3C_2T_x$). Here, Rh catalyzes H_2O_2 decomposition while Ru generates $^1O_2$ under NIR; the system enhances H_2O_2 adsorption and charge transfer, synergizing catalytic performance. The RhRu/$Ti_3C_2T_x$ platform provides a more effective and safer therapeutic strategy for OS, representing an integrated approach combining PDT, PTT, and CDT (**Figure 5A**).

Although promising 2D materials like MXenes have high photothermal/ROS potential,[68] their efficacy is hampered by hypoxia. Zheng et al.[69] addressed this via a CeO_2@MXene Schottky heterojunction, where CeO_2 catalyzes tumor H_2O_2 for self-oxygenation. This integrates Type I/II PDT synergism, MXene's PTT, enhanced charge separation, and Ce^{3+}/Ce^{4+} redox cycling for intelligent oxygen modulation, improving PDT outcomes with superior tumor penetration. Additionally, Gu et al.[70] tackled hypoxia using Pd@Pt core–shell nanocomposites (Pd@Pt-PEG), where the ultrathin Pt shell enhances charge accumulation and offers dual PTT/PDT. These efficiently catalyze tumor H_2O_2 to generate oxygen, alleviating hypoxia and augmenting PDT (Figure 5B). Surface PEGylation prolonged circulation and enabled imaging guidance.

Bismuth-based nanomaterials show promise for imaging-guided PTT/PDT, but face fabrication and translation challenges. Cheng et al.[71] synthesized Tween-20-modified $AgBiS_2$ nanoparticles showing high photothermal efficiency (36.51% @ 808 nm), enhanced H_2O_2 consumption/ROS generation, and synergistic PTT/PDT against OS (Figure 5C), integrating therapy, imaging, and anti-infection.

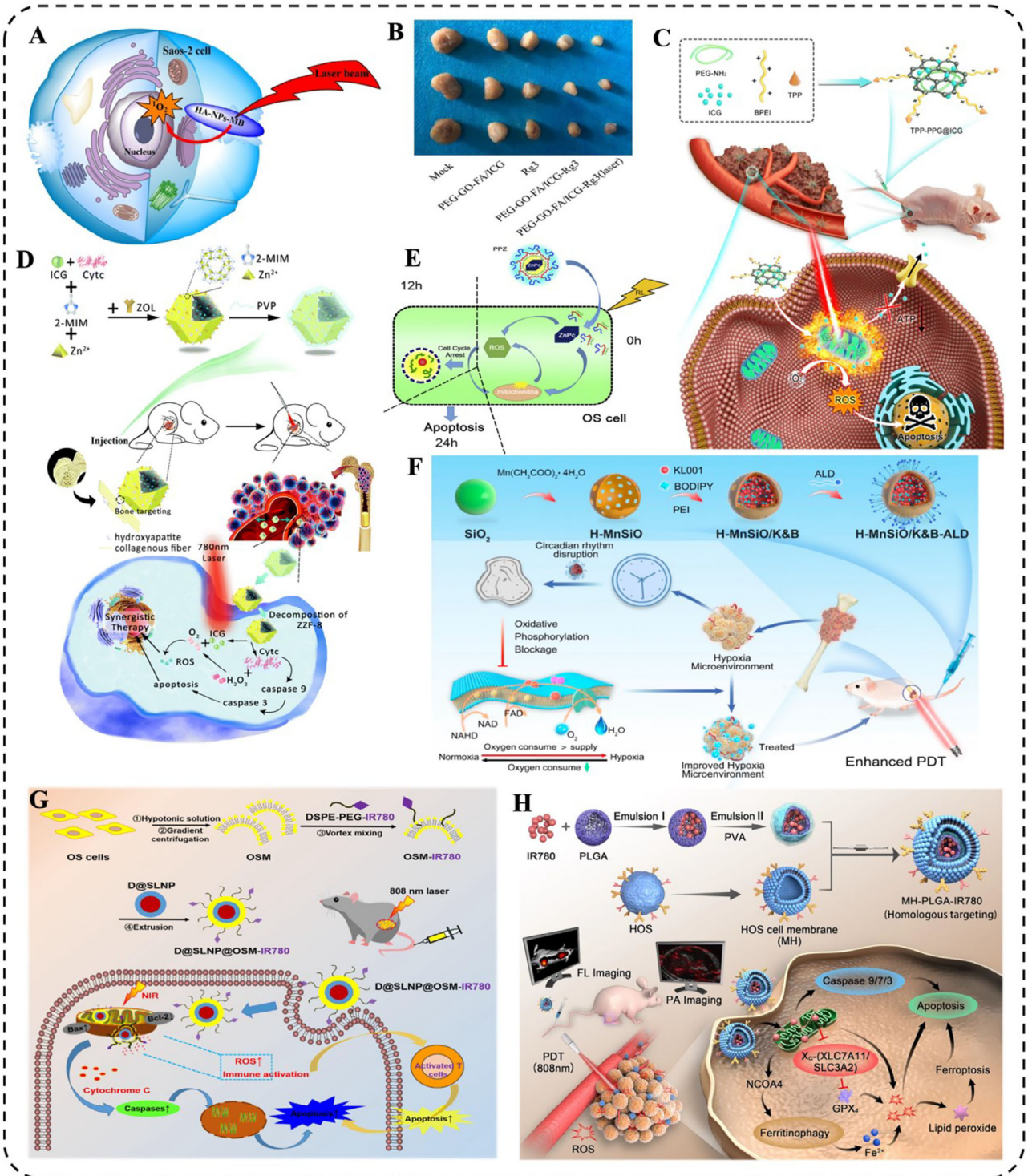

Figure 4. Dye-based PS combined with nanocarriers: Overcoming tumor hypoxia and drug resistance. A) Mechanism of $^1O_2$ generation by HA-NPs-MB/laser in osteosarcoma cells. Reproduced with permission.[56] Copyright 2020, Elsevier. B) Ex vivo tumor images in nude mice. Reproduced with permission.[57] Copyright 2021, Frontiers. C) Mitochondrion-targeting TPP-PPG@ICG nanocomposite for single-laser synergistic phototherapy. Reproduced with permission.[58] Copyright 2021, Springer Nature. D) Synthesis and bone-targeting synergistic therapy of ICG/Cyt c@ZIF-8@PVP NPs. Reproduced with permission.[59] Copyright 2022, Royal Society of Chemistry (RSC). E) ZnPc release via PPZ NPs degradation in OS cells. Reproduced with permission.[61] Copyright 2018, Elsevier. F) $MnSiO_3$/K&B-ALD nanoparticles for enhanced osteosarcoma photodynamic therapy. Reproduced with permission.[63] Copyright 2023, Elsevier. G) Antitumor mechanism and preparation of D@SLNP@OSM-IR780 NPs. Reproduced with permission.[64] Copyright 2024, Elsevier. H) MH-PLGA-IR780 nanoplatform-mediated targeted PDT killing mechanism. Reproduced with permission.[65] Copyright 2022, Springer Nature.

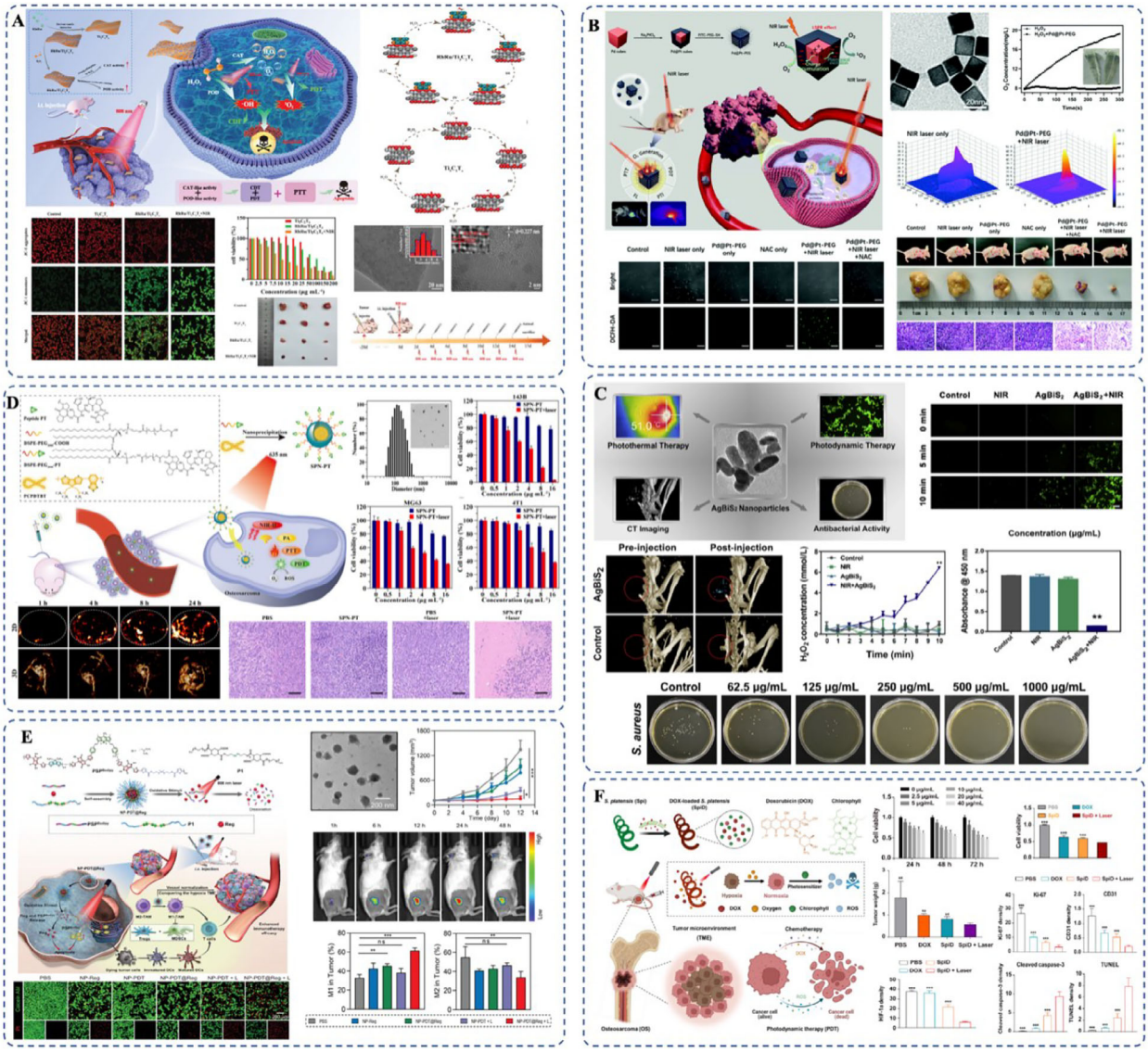

Figure 5. Alternative PDT strategies for bone malignancies. A) Bimetallic RhRu nanozyme ($RhRu/Ti_3C_2T_x$). Reproduced with permission.[67] Copyright 2023, Wiley-VCH. B) Pd@Pt core–shell nanocomposite with catalase-mimicking activity and photothermal/photodynamic dual-modal functions (Pd@Pt-PEG). Reproduced with permission.[70] Copyright 2021, Royal Society of Chemistry (RSC). C) $AgBiS_2$ nanoparticles enabling PTT/PDT dual-modal therapy. Reproduced with permission.[71] Copyright 2020, Elsevier. D) PT oligopeptide-targeted semiconductor polymer nanoparticles (SPN-PT). Reproduced with permission.[73] Copyright 2022, Springer Nature. E) NIR-II-responsive degradable quasi-conjugated polymeric system (NP-PDT@Reg). Reproduced with permission.[75] Copyright 2023, Wiley-VCH. F) Spirulina (Spi)-based drug delivery system (SpiD). Reproduced with permission.[76] Copyright 2024, American Chemical Society (ACS).

Overcoming PDT's shallow penetration depth (<2 mm) and NIR limitations (high power, low quantum yield), Zhang et al.[72] developed NIR-activated $NaYbF_4$ nanoparticles. These generate $^1O_2$ efficiently under 980 nm excitation via $Yb^{3+} \rightarrow O_2$ linear energy transfer (1.27 eV → 0.97 eV), enabling real-time laser/oxygen monitoring and precise regulation for deep-tissue PDT.

Semiconductor Photosensitizers Demonstrate Promising Therapeutic Potential: Recent advances in PDT have highlighted semiconductor-based photosensitizers as pivotal research targets. Yuan et al.[73] developed osteosarcoma-targeted semiconducting polymer nanoparticles (SPN-PT) via nanoprecipitation of PEG-PT-conjugated PCPDTBT (Figure 5D). This platform synergizes NIR-II fluorescence/NIR-I photoacoustic imaging, with PT peptide-mediated uptake enhancing early detection sensitivity. Under 808 nm irradiation, SPN-PT delivered concurrent photothermal/photodynamic activity, demonstrating preclinical promise as a precision theranostic agent

While π-conjugated polymers show PDT potential,[74] non-degradability hampers clinical translation. To address this, Wan et al. engineered a tumor-responsive pseudo-conjugated system (PSP^{Bodipy}) activated by NIR-II light.[75] Their NP-PDT@Reg nanoplatform co-assembled diselenide polymers and regorafenib, enabling light-triggered drug release, vascular remod-

eling for hypoxia alleviation, and p38/Creb1/Klf4-mediated immunosuppression reversal (Figure 5E). This amplified M1 polarization (1.2–2× $CD8^+$ T-cell infiltration), depleted Tregs/MDSCs (≤25–40% baseline), and induced robust immunogenic cell death. The synergistic strategy represents a transformative advance in dismantling microenvironmental resistance mechanisms underlying osseous malignancies.

Natural Biomaterials for PDT: In contrast to synthetic materials, natural biomaterials are increasingly recognized as alternatives to synthetic platforms in oncotherapy. Microalgae-derived systems exemplify this trend, with An et al.[76] reporting a spirulina-based nanocomposite (SpiD) for dual chemo-photodynamic osteosarcoma treatment. Spirulina's photosynthetic O_2 generation under 650 nm light alleviated hypoxia while amplifying chlorophyll-mediated ROS, synergizing with pH-responsive doxorubicin release for effective osseous tumor suppression (Figure 5F).

Meanwhile, phytochemical optimization studies demonstrated aloe-emodin (AE)-PDT's tumor-selective cytotoxicity at submutagenic doses (10 μM, 4.8 J cm^{-2})[77] through mitochondrial/ER-targeted ROS-JNK signaling.[78] Parallel efforts addressed *Cichorium pumilum*'s pharmaceutical limitations, with Makhadmeh et al.[79] demonstrating silica nanoencapsulation (CP-SiNPs) enhanced both aqueous stability and photodynamic potency, enabling effective tumor clearance at reduced dosages and irradiation durations.

3.2. SDT in Bone Tumors: Deep-Tissue Penetration and Immunogenic Cell Death

3.2.1. SDT with Metalloporphyrins: Sono-Immunotherapy and Apoptotic Signaling

As previously, mentioned, hematoporphyrin and its derivatives, as classical PSs, demonstrate significant potential in SDT, with representative compounds including Hp, PpIX, and HMME. Hp combined with ultrasound elicits synergistic antitumor effects through multiorganelle damage, including membrane dysfunction, enzyme inhibition, mitochondrial swelling, and chromatin condensation.[80,81] Hp-SDT generates $^1O_2$ via mitochondrial-localized Hp, activating caspase-8/9-PARP cascades and inducing apoptosis through cytochrome-C translocation and Bax upregulation.[80–82]

Similarly, HMME targets mitochondrial pathways under ultrasound, activating caspase-9/caspase-3 cascades while upregulating Bax and suppressing Bcl-2.[83] PpIX demonstrates superior efficacy versus Hp;[84] PpIX-SDT enhances apoptosis via Fas/caspase-8/-3 signaling and induces PARP cleavage/DNA fragmentation.[85] Ultrasound further accelerates PpIX aggregation while promoting its decomposition to amplify Fenton reactions (generating ·OH/$\cdot O_2^-$), elucidating the oxidative damage mechanism.[86]

5-ALA-derived PpIX localizes in mitochondria, where ultrasound-generated ROS induces apoptosis via mitochondrial membrane potential collapse, Bcl-2 downregulation, and Bax/p53/caspase-3 upregulation.[87] Sinoporphyrin sodium (DVDMS) exhibits robust ultrasound-activated antitumor effects through mitochondrial apoptosis (caspase-3/9 activation, PARP cleavage) while suppressing PCNA/VEGF.[88] Tumor-targeted DVDMS accumulation peaks under triple ultrasound irradiation (2/6/24 h post-administration), achieving 1.6-fold higher suppression versus single-dose treatment without thermal damage or metastatic risk.[89]

3.2.2. Catalytic Nanoreactors for SDT: Piezoelectric Fenton Reactions and ROS Cascades

ICG and MB were previously proposed as dye-based photosensitizers applicable to SDT. However, studies revealed that ICG-SDT predominantly relies on photodynamic effects, where US merely enhances efficacy without playing a dominant role.[90] In contrast, MB-SDT is governed by sonodynamic effects, as US-activated MB eliminates tumor cells via hydroxyl radical-dominated ROS-mediated cytotoxicity.[91]

Currently, PD-1/PD-L1 immunotherapy achieves a response rate of only 5%, while the CD47 inhibitor RRx-001 shows promise by suppressing tumor immune evasion. Gong et al.[92] thus developed a biomimetic nanodrug (MPIRx) using a polyethylene glycol-polycaprolactone (PEG-PCL) copolymer to co-load RRx-001 and the sonosensitizer IR780, cloaked with osteosarcoma cell membranes for enhanced targeting. This system synergized CD47 blockade with SDT, significantly suppressing orthotopic osteosarcoma growth and lung metastasis (**Figure 6A**). The strategy provides a novel approach for osteosarcoma sonodynamic/immunotherapy, integrating targeted delivery and microenvironment modulation.

Traditional nanocarriers depend on the enhanced permeability and retention effect and passive drug release via self-degradation, posing off-target risks. Zhou[93] designed ultrasound-triggered liposomes (NGR/UT-L) incorporating the CD13-targeting peptide NGR, the sonosensitizer Ce6 ester, and doxorubicin (DOX) (Figure 6B). This platform combines SDT with spatiotemporally controlled drug delivery, overcoming the tissue penetration limits of phototherapy. It offers a novel strategy for deep-seated tumors (e.g., osteosarcoma) with high tissue penetrability, minimal systemic toxicity, and active targeting capabilities.

3.2.3. Bioengineered SDT Platforms: Stem Cell Carriers and Biomimetic Targeting

Compared to conventional sonosensitizers (e.g., porphyrins), ultrasound-responsive nanomaterials show superior potential due to tunable size/morphology/surface properties that enhance biocompatibility and biodistribution. Zlotver[94] designed glucose-modified TiO_2/polymer hybrids (glu-aTiO_2/PEO-PPO) for targeted SDT (Figure 6C). Precise size control (30–300 nm) and glycosylation enabled GLUT-1-targeted accumulation in rhabdomyosarcoma, significantly prolonging survival in tumor models.

To overcome TME limitations (inadequate H_2O_2/GSH), Geng et al.[95] synthesized W-doped TiO_2 nanorods. PEG modification enhanced dispersibility, while bandgap reduction (3.2→2.3 eV) amplified ultrasound-triggered ROS. The nanoparticles synergized CDT/SDT via ·OH generation and GSH depletion (Figure 6D). Ferroptosis induction complements SDT for hypoxia resistance. Sun et al.[96] constructed Fe-porphyrin MOFs

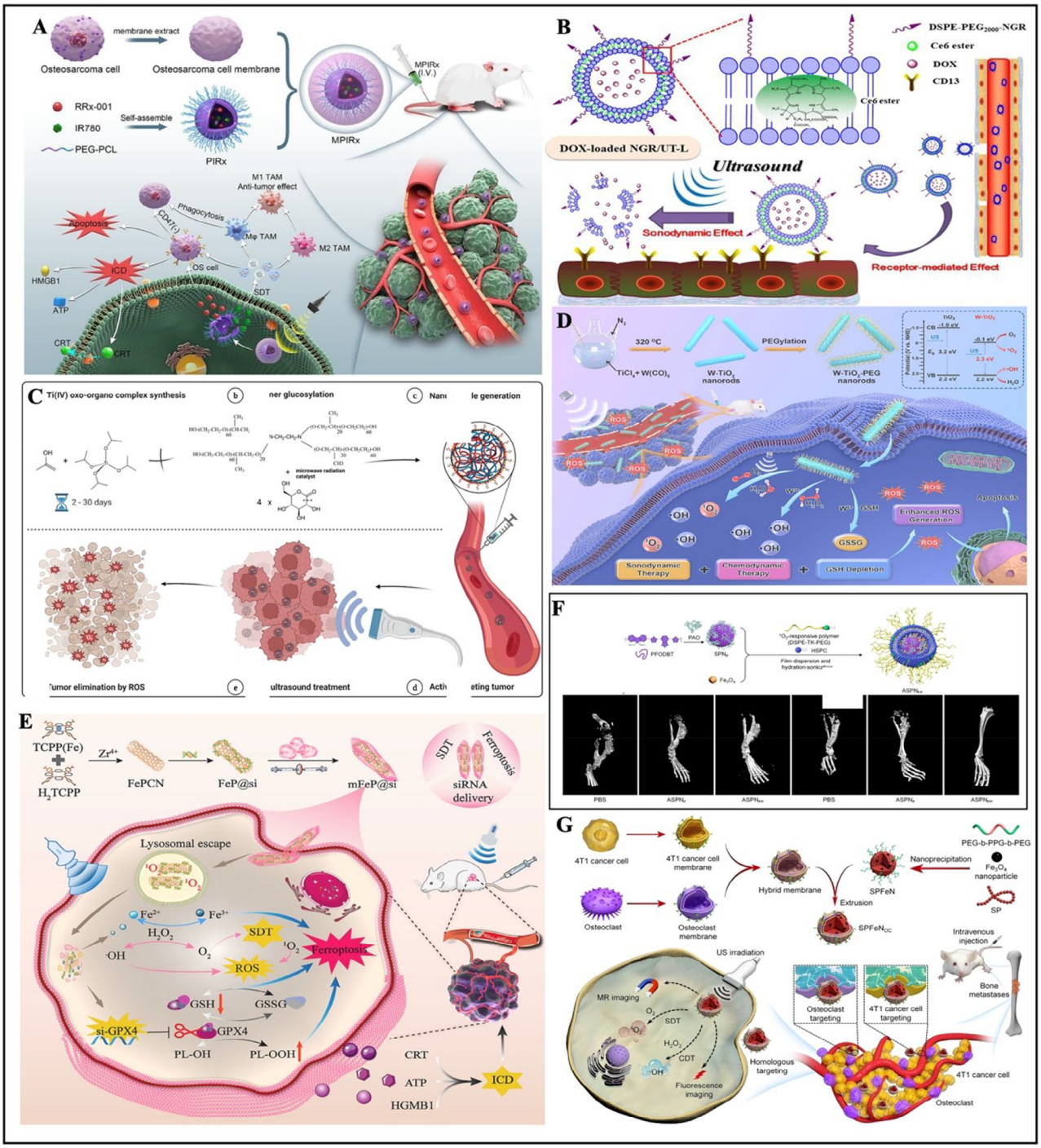

Figure 6. Sonosensitizers and nanocarriers in bone tumor treatment. A) Mechanism and assembly of MPIRx nanodrugs for CD47 immune checkpoint/sonodynamic therapy in osteosarcoma with lung metastasis. Reproduced with permission.[92] Copyright 2023, Elsevier. B) DOX-loaded NGR/UT-L system schematic. Reproduced with permission.[93] Copyright 2019, American Chemical Society (ACS). C) Synthesis and sono-responsive performance of glu-aTiO$_2$/PEO-PPO nanomaterials. Reproduced with permission.[94] Copyright 2023, Wiley-VCH. D) Ultrafine W-TiO$_2$ nanorods fabrication with TME-regulating capacity for CDT-augmented SDT. Reproduced with permission.[95] Copyright 2021, American Chemical Society (ACS). E) Synthesis pathway and mechanistic overview of mFeP@st nanoparticles. Reproduced with permission.[96] Copyright 2024, Elsevier. F) Preparation and potent in vivo antitumor efficacy of ASPNFP. Reproduced with permission.[23] Copyright 2023, American Chemical Society (ACS). G) SPFeNOC construction via nanoprecipitation/cell membrane camouflage and dual-targeting strategy for amplified bone metastasis theranostics. Reproduced with permission.[97] Copyright 2023, Wiley-VCH.

(mFeP@si) for GPX4-targeted siRNA delivery. pH-responsive siRNA release silenced GPX4, while US-activated ROS and GSH depletion induced ferroptosis and ICD, remodeling the TME and restoring cisplatin sensitivity (Figure 6E).

Zhang's semiconducting polymer nanoinducer (ASPNFP)[23] utilized Fe_3O4-loaded carriers where ultrasound-triggered ROS initiated Fe_3O4 release, amplifying ·OH via Fenton effects. Concurrent PAO-catalyzed polyamine decomposition synergistically enhanced oxidative damage (Figure 6F). Their SPFeNOC system[97] achieved dual tumor/osteoclast targeting via hybrid membranes, enabling NIR/MR imaging-guided therapy (Figure 6G). Yumita et al.[98] confirmed PEG-functionalized CNTs as potent sonosensitizers through $^1O_2$ generation.

4. Bone Infectious Disease

Bone infections, caused by pathogens like bacteria or fungi, form deep inflammatory lesions beneath the skin. Conventional systemic pharmacotherapy often fails to penetrate deep tissues effectively, limited by poor targeting, adverse effects, and rising drug resistance. These challenges require novel therapies. PDT activates PS to generate ROS for precise pathogen killing, offering enhanced targeting and minimal risk of microbial resistance, positioning it as a potential replacement for chemotherapy.[99] However, SDT is emerging to overcome PDT's poor tissue penetration and combat antibiotic resistance.

4.1. PDT in Bone Infectious Disease: Antibiofilm and Immunoadjuvant Approaches

4.1.1. PDT with Hematoporphyrins: Bacterial Membrane Disruption and Oxygen Self-Supply

Hematoporphyrin-based PS, including 5-ALA and PpIX, have been utilized in treating bone infectious diseases such as osteomyelitis. Notably, studies report significant reduction in osteomyelitic lesions and marked suppression of biofilm growth following transdermal 5-ALA-PDT administration.[100] However, standalone use of porphyrin-based PS like 5-ALA faces limitations such as suboptimal efficacy and poor biocompatibility. Consequently, the development of high-efficiency, multifunctional nanoparticles has emerged as a research priority. Pan et al.[101] developed vancomycin-modified graphene oxide quantum dots/PpIX (Van-GQDs/PpIX) nanocomposites (Figure 7A). Van confers bacterial cell wall targeting while GQDs: i) co-load Van/PpIX; ii) enhance targeted delivery; iii) create additional Van-binding sites; and iv) amplify X-ray activation (2 Gy, 6 MV) for efficient pathogen eradication at low radiation doses. This strategy offers a low-radiation, high-targeting therapeutic approach for deep-seated infections like osteomyelitis, though in vivo safety and broad-spectrum antimicrobial efficacy require further validation.

LD40, a novel photosensitizer, belongs to the class of base-amino-acid-modified aminophenyltetraporphyrin compounds. Yin et al.[102] evaluated LD4-mediated PDT combined with low-dose gentamicin for treating methicillin-resistant *Staphylococcus aureus* (MRSA)-induced tibial osteomyelitis in rabbits. While this study proposes a novel strategy for drug-resistant osteomyelitis, further investigations are needed to assess its applicability against other pathogens and clinical translation feasibility.

4.1.2. Dye-Based PDT Systems: ICG-Loaded Nanocarriers and Synergistic Antibiotics

Dye-based PS such as ICG and toluidine blue have been widely used in PDT for bone infectious diseases. Toluidine blue-PDT (5 μg mL^{-1}, 660 nm laser) inhibits *S. aureus* growth[103] and controls osteomyelitis in animal models.[104]

The development of multifunctional and highly targeted therapeutics has gained substantial attention. Lu et al.[105] engineered BMUIG nanoparticles (bovine serum albumin-MnO_2-UBI29-41-ICG-gentamicin) achieving dual-modal imaging (ICG-mediated photoacoustic + MnO_2-enhanced MRI, $r_1 = 6.06$ мм$^{-1}$ с$^{-1}$) and synergistic therapy (**Figure 7B**). UBI29-41 peptide enables bacterial targeting, while acidic TME-activated MnO_2 catalyzes oxygen generation to amplify ICG-PDT, combined with low-dose gentamicin (0.5 μg mL^{-1}).

Clinical allograft implants are highly susceptible to bacterial biofilm colonization (e.g., by *S. aureus*), leading to implant-associated infections (IAIs), which often fail conventional antibiotic therapies due to pathogen resistance. Post-biofilm formation, the physical barrier created by extracellular polymeric substances impedes immune cell infiltration and antimicrobial penetration, frequently necessitating revision surgery. Yuan et al.[106] designed a Ti-M/I/RGD implant coating (Figure 7C). Mesoporous polydopamine nanoparticles co-load ICG and covalently conjugate RGD peptides, enabling simultaneous PDT/PTT bacterial elimination and RGD-mediated osteogenesis—providing a non-invasive solution to biofilm-related IAIs.

4.1.3. Biofilm-Smart PDT: pH-Responsive ROS Burst and Extracellular Matrix Degradation

IAIs often exhibit persistent and recurrent characteristics due to hypoxic and acidic microenvironments as well as immunosuppressive factors (e.g., regulatory T cells, Tregs) that inhibit immune responses. To address this refractory issue, Jiang et al.[107] addressed this by developing a photo-immunomodulatory nanoplatform (BMCV) targeting *Staphylococcus aureus*-induced IAIs (Figure 7D). MnO_2 catalyzes H_2O_2-to-oxygen conversion in acidic conditions to amplify Ce6-PDT efficacy, while ROS-mediated extracellular DNA degradation disrupts biofilm integrity. This strategy simultaneously reverses biofilm-immunosuppressive microenvironments in drug-resistant infections.

Existing PDT strategies primarily focus on bactericidal stages, lacking dynamic regulation of the TME during subsequent bone repair. Xie et al.[108] engineered a peptide-derived bilayer hydrogel (AA-MAR) for osteomyelitis (Figure 7E). The system enables spatiotemporally controlled release: the upper layer's photosensitizer eliminates pathogens and induces macrophage M1 polarization, while the lower layer's BMSCs promote osteogenesis and macrophage M2 reprogramming. This integrates antibacterial action, immunomodulation, and bone regeneration within a

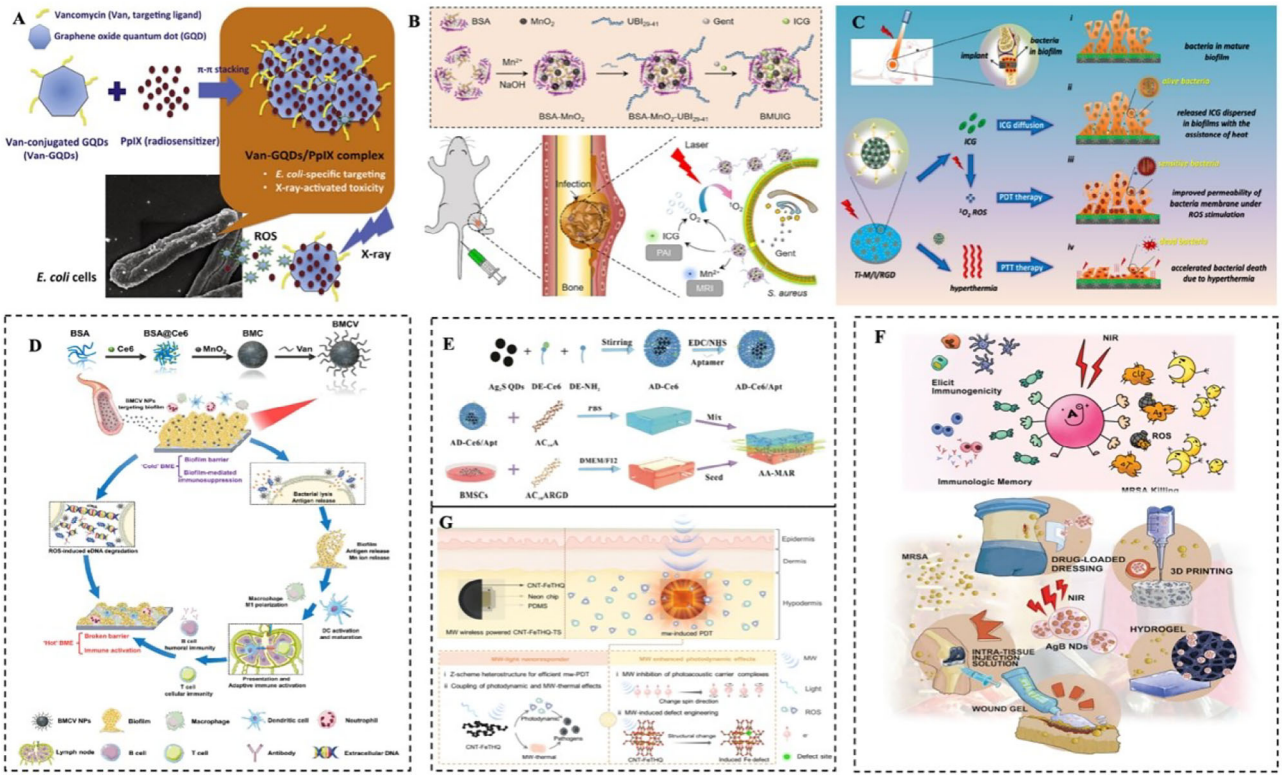

Figure 7. PDT applications in bone infectious diseases. A) Synthesis pathway and mechanistic overview of Van-GQDs/PpIX nanocomposite. Reproduced with permission.[101] Copyright 2016, Elsevier. B) BMUIG preparation for dual-modality imaging/phototherapy in osteomyelitis management. Reproduced with permission.[105] Copyright 2019, Elsevier. C) NIR-triggered remote-controlled PDT/PTT synergy eliminating pre-existing *S. aureus* biofilms on Ti-M/I/RGD implants. Reproduced with permission.[106] Copyright 2019, Elsevier. D) BSA@MnO_2@Ce6@Van (BMCV) nanoplatform. Reproduced with permission.[107] Copyright 2024, American Chemical Society (ACS). E) Composition pathway of AD-Ce6/Apt and AA-MAR structural schematic. Reproduced with permission.[108] Copyright 2022, Springer Nature. F) AgB NDs for postoperative infection control with promising clinical translation potential. Reproduced with permission.[111] Copyright 2022, Wiley-VCH. G) MW-wirelight neon chip-powered mw-PDT platform. Reproduced with permission.[112] Copyright 2024, American Chemical Society (ACS).

single platform. This study proposes an innovative strategy integrating PDT-mediated antibacterial activity, immunomodulation, and bone repair for osteomyelitis management.

4.1.4. Alternative PDT Strategies

Biofilm-Smart PDT: pH-Responsive ROS Burst and Extracellular Matrix Degradation: Fullerenes (C60), with their unique sp^2-carbon structure and ROS-generating capacity, are promising photosensitizers; however, their hydrophobicity limits practical applications. Hydroxylated fullerols (C60(OH)30) overcome this, eliminating MRSA under NIR femtosecond laser irradiation (228.8 nJ pixel^{-1}) via two-photon absorption ($\sigma = 1187.5$ GM).[109] Generating $^1O_2$ and $O_2{\cdot}^-$, they achieve complete bacterial inactivation within 3.67 s. Hydroxylation enhances aqueous solubility (particle size: 1.05 ± 0.02 nm) and biocompatibility, with TEM confirming membrane damage and DNA oxidation. This work demonstrates a novel nanophotosensitizer strategy for deep-tissue drug-resistant infections.

Organic room-temperature phosphorescent (RTP) materials, which generate abundant triplet excitons, are potential photosensitizers, though their photodynamic mechanisms remain unclear. Chao et al.[110] developed a host-guest system (BP/BQD) using microfluidics to control NP size (105–220 nm) and crystallinity. This redirects triplet exciton decay toward ROS generation, synergizing Type I/II reactions with 20× accelerated ROS production for low-toxicity PDT in deep-tissue infections.

Metal-Functionalized Nanoparticles Facilitate Enhanced Photodynamic Osteomyelitic Therapy: Postoperative MRSA infections pose significant clinical challenges due to high recurrence and mortality rates, as conventional debridement and vancomycin fail to eradicate biofilm-resident bacteria or activate immune surveillance. Tang et al.[111] created BSA-stabilized Ag-S quantum dots (AgB NDs, Figure 7F). Under NIR, they synergistically release Ag^+, generate ROS, and provide photothermal effects while dysregulating bacterial genes (upregulated heat shock/antioxidant genes; downregulated virulence/biofilm genes). Treatment accelerated healing, reduced inflammation (CRP/IL-6), and induced immunogenic cell death to establish immune memory.

Microwave (MW)-induced photodynamic therapy (mw-PDT) was proposed to overcome limitations in deep-tissue infection treatment, such as insufficient laser penetration and antibiotic resistance. While MW offers superior tissue penetration, its energy alone cannot directly generate ROS. Qiao et al.[112] synthesized a dual-responsive material, CNT-FeTHQ (carbon nanotubes/iron-

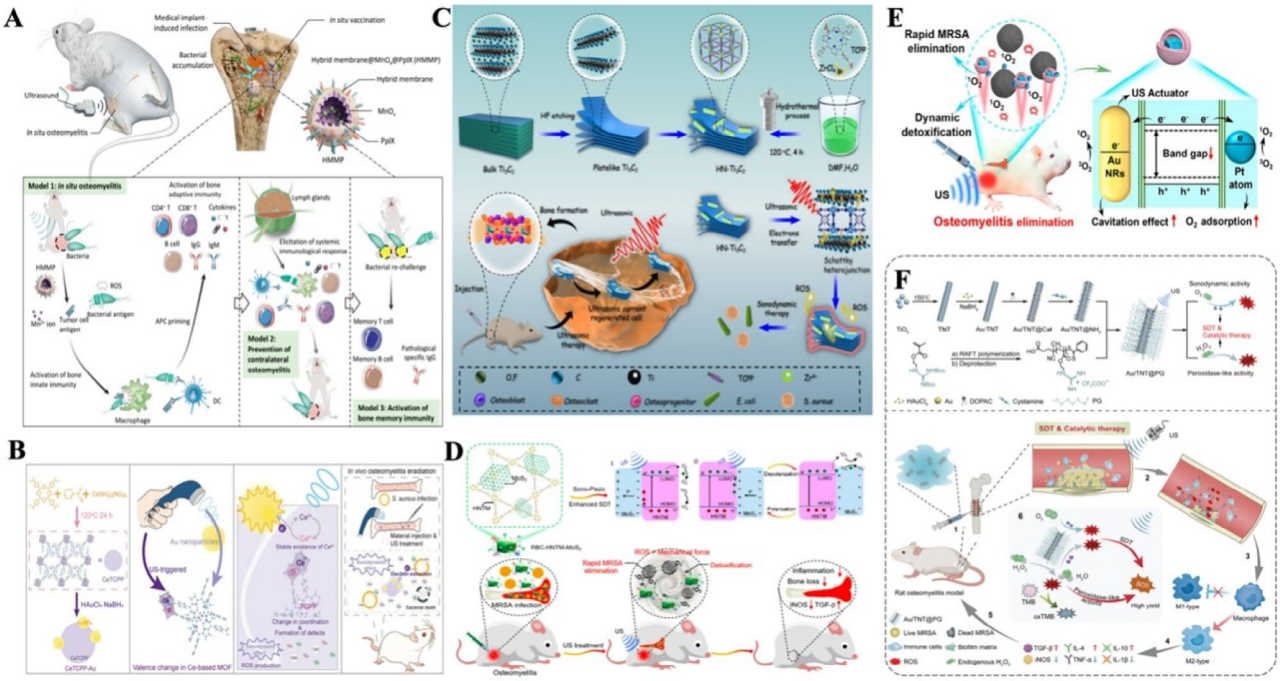

Figure 8. SDT-based therapy for osteomyelitis management. A) Immunostimulatory HMMP-based nanovaccine for in situ osteomyelitis immunotherapy. Reproduced with permission.[114] Copyright 2022, American Chemical Society (ACS). B) Defect-engineered CeTCPP-Au sonosensitizer for enhanced SDT against osteomyelitis via ultrasound-activated electron trapping. Reproduced with permission.[118] Copyright 2023, Wiley-VCH. C) Mechanistic pathway of sonodynamic therapy for *S. aureus*-infected osteomyelitis disruption. Reproduced with permission.[19] Copyright 2023, Ivyspring International Publisher. D) HNTM-MoS_2-driven sonocatalytic detoxification and MRSA elimination in SDT-targeted osteomyelitis treatment. Reproduced with permission.[120] Copyright 2022, American Chemical Society (ACS). E) RBC-HNTM-Pt@Au nanocatalyst for biofilm-penetrating sonodynamic eradication of osteomyelitis. Reproduced with permission.[121] Copyright 2021, American Chemical Society (ACS). F) Au/TNT@PG nanostructure-mediated dual-function therapy. Reproduced with permission.[124] Copyright 2022, Wiley-VCH.

based conductive metal-organic framework). The wireless platform (CNT-FeTHQ-TS) activates neon lamps via microwaves, achieving 99.63% bactericidal efficacy against *S. aureus* through combined photothermal/photodynamic effects with excellent biocompatibility (Figure 7G).

For IAIs, Wang et al. synthesized PEG-modified Cu9S8 nanoparticles via one-step wet chemistry.[113] Under NIR excitation, Cu9S8 synergized PTT and PDT effects to continuously generate ROS, including $^1O_2$ and hydrogen peroxide, causing bacterial membrane rupture and genomic DNA damage. Crucially, the material exhibited favorable biocompatibility in vivo, underscoring its potential for clinical translation.

4.2. SDT in Bone Infectious Disease: Mechanical Biofilm Rupture and Dynamic Defense

4.2.1. SDT with Porphyrins Sensitizers: Nanozyme-Mediated Bacterial Lysis

Single-component hematoporphyrin-based compounds are rarely applied in SDT for osteomyelitis, often integrated into multifunctional nanoparticles. Lin et al.[114] developed a biomimetic nanovaccine, HMMP (macrophage/tumor cell membrane-fused MnOx@PpIX), which triggers explosive ROS release via SDT to eliminate bacteria and release broad-spectrum antigens, offering a dual-functional strategy combining localized sterilization and systemic immune activation for osteomyelitis (**Figure** 8A). The MnOx core decomposes in the infected microenvironment (IME) to generate oxygen, enhancing the SDT efficacy of PpIX. Concurrently, the tumor cell membrane acts as an immune adjuvant, synergizing with Mn^{2+} to promote DC maturation and macrophage M1 polarization. Notably, HMMP induced long-term memory immunity, providing sustained protection against reinfection.

A dual-functional sonosensitizer composed of porphyrin-like Zn single-atom catalysts (g-ZnN4) and MoS2 quantum dots (g-ZnN4-MoS2) was reported to integrate efficient antibacterial activity and osteogenic promotion.[115] Feng et al. constructed heterointerfaces to facilitate charge separation under ultrasound, reducing the activation energy of O_2 and significantly enhancing $^1O_2$ yields, achieving a 99.58% antibacterial rate against MRSA in vitro. Moreover, the sustained release of Zn^{2+} (<5 mg L^{-1}) at safe concentrations promoted osteogenic gene expression (ALP, RUNX2, COL-I). This strategy provides a multifaceted, low-toxicity solution for SDT in bone infectious diseases.

4.2.2. Ultrasound-Activated Nanomotors: Physical Disruption of Antibiotic Resistance

To improve the targeting precision of the dye-based photosensitizer IR780, Chen et al.[116] developed M2 macrophage

membrane-coated PLGA NPs (M2/IR780@PLGA) against MRSA. The M2 membrane enables inflammatory targeting, while subsequent ultrasound (1 MHz, 2 W cm^{-2}) triggers IR780-generated $^1O_2$. This synergy potently inhibited MRSA growth and eradicated biofilms. With demonstrated biocompatibility, this system constitutes a precision sonodynamic-immunomodulatory strategy for resistant MRSA infections.

Hospital-acquired MRSA osteomyelitis treatment is challenged by insufficient deep-drug delivery and MRSA-driven immunosuppression. A sonodynamic immunotherapeutic nanovesicle, VCG@MMW, was developed to address this.[117] It uses mannose-grafted M1 macrophage microvesicles for targeted delivery. These vesicles carry vancomycin-crosslinked micelles containing ICG. In models, VCG@MMW enhanced survival, induced M1 macrophage polarization, activated T-cells, bolstered defense against primary and homologous transferred MRSA infections, improved clearance, and reduced recurrence risk. This strategy combines targeted delivery, sonodynamic therapy, and immune reprogramming for deep MRSA infections.

4.2.3. Alternative SDT Strategies

Metal-organic frameworks (MOFs), pivotal porous compounds formed by metal ions/clusters connected via organic linkers to create tunable 3D architectures, offer promising platforms for developing high-performance sensitizers.

Zheng et al.[118] proposed a novel strategy for designing MOF-based sonosensitizers via dynamic defect engineering. Their cerium-based MOF (CeTCPP) integrated with in situ reduced gold nanoparticles (CeTCPP-Au) demonstrated potent anti-MRSA osteomyelitis activity (Figure 8B). The CeTCPP-Au/US combination exhibited potent bactericidal effects against *S. aureus* and *E. coli*, reduced systemic IL-6 levels, and diminished inflammatory cell infiltration. Similarly, Zeng developed a defective homojunction porphyrinic MOF (D-PCN-2) for MRSA osteomyelitis by modulating the crystallization of PCN-222 using acetic acid as a modulator, forming an integrated PCN-222/PCN-224 heterostructure.[119] Under US activation, D-PCN-2 effectively suppressed MRSA proliferation, disrupted bacterial membranes, reduced inflammatory cell infiltration at infection sites, and promoted macrophage M2 polarization

Porphyrinic MOFs, exemplified by hollow nanotubular metal-organic frameworks (HNTMs), represent another 3D scaffold. Building on this, Wang et al.[19] engineered an HNTM-Ti_3C_2 MXene Schottky heterojunction (HN-Ti_3C_2; Figure 8C), where Ti_3C_2 enhanced US-driven charge separation in HNTM, amplifying ROS generation and MRSA inhibition. Low-intensity US (1.5 W cm^{-2}) further activated Ca^{2+}/Wnt pathways, promoting BMSC osteogenesis via cell cycle/DNA replication/apoptosis regulation, though targeting efficacy requires optimization. Additionally, Feng et al.[120] developed RBC-HNTM-MoS_2 (Figure 8D) by electrostatically anchoring MoS_2 onto HNTM; US-polarized MoS_2 augmented HNTM's sonocatalysis for potent ROS production while disrupting bacterial membrane integrity via metabolic interference. The RBC-coating enhanced biocompatibility, enabling erasure of deep infections, inflammation attenuation, M2 macrophage polarization, bone loss reduction, and accelerated regeneration post-US (1.5 W cm^{-2}). Meanwhile, Yu et al.[121] constructed RBC-HNTM-Pt@Au (Figure 8E) with Pt atoms (bandgap reduction, enhanced O_2 adsorption) and Au nanorods, which significantly lowered pro-inflammatory cytokines, induced M2 polarization, and preserved bone volume. Collectively, these studies establish antibiotic-free sonodynamic platforms for deep bone infection management.

Current research efforts are actively exploring innovative sonosensitizers. Some researchs reported that emodin (EM) is one kind of efficient sonosensitizers.[122] Li et al. incorporated EM into Mn-doped TiO_2 nanorods (ED-TOM),[123] where sonogenerated ROS synergistically disrupt bacterial membranes, accelerate Mn^{2+} uptake to induce ferroptosis-like effects, and promote M2 polarization with osteogenic differentiation. In parallel, Cheng et al.[124] engineered Au/TNT@PG nanoparticles by functionalizing Au-doped titanate nanotubes (Au/TNT) with guanidine-rich polymers (PG) to target MRSA biofilms (Figure 8F). Here, Au/TNT acts as a US-responsive scaffold while PG enhances biofilm penetration. The nanoparticles exhibit peroxidase-mimicking activity under US irradiation, augmenting SDT via $^1O_2$ generation. They concurrently attenuate pro-inflammatory cytokines (TNF-α/IL-1β) and elevate anti-inflammatory cytokines (IL-4/IL-10) in bone tissue. With demonstrated biosafety, this platform offers enhanced efficacy against deep biofilm infections.

5. Degenerative Metabolic Bone Diseases

5.1. PDT in Degenerative Bone Disorders: Synovial Fibroblast Ablation and Cartilage Preservation

Research on the applications of PDT in degenerative and metabolic bone disorders has been relatively understudied compared to its use in bone tumors and infectious bone diseases. This review focuses on the therapeutic potential of PDT in conditions such as rheumatoid arthritis (RA) and osteoarthritis (OA).

5.1.1. Rheumatoid Arthritis Management

RA, the most common chronic inflammatory disease, is characterized by persistent synovitis, irreversible joint destruction, and progressive disability. Current clinical management relies on DMARDs, NSAIDs, and glucocorticoids to attenuate disease progression. However, chronic administration of these agents is associated with severe complications, including myelosuppression and hepatic impairment. PDT, particularly in combination with chemotherapeutic regimens, has emerged as a promising alternative strategy to address these limitations.

Natural PS for RA-PDT: Enhanced Permeability and Biosafety: Hypericin (HYP), a naturally occurring polycyclic phenanthroperylenequinone isolated from *Hypericum perforatum*, represents one of the most potent photosensitizers capable of selectively inducing apoptosis in RA fibroblast-like synoviocytes (RA-FLS).[125,126] Leveraging this property, Abd-El-Azim et al.[127] pioneered a microneedle-enhanced PDT approach utilizing HYP-loaded emulsomes (HYP-EMLs) delivered via hollow microneedles (Ho-MNs, 1200 μm; AdminPen system) for RA treatment

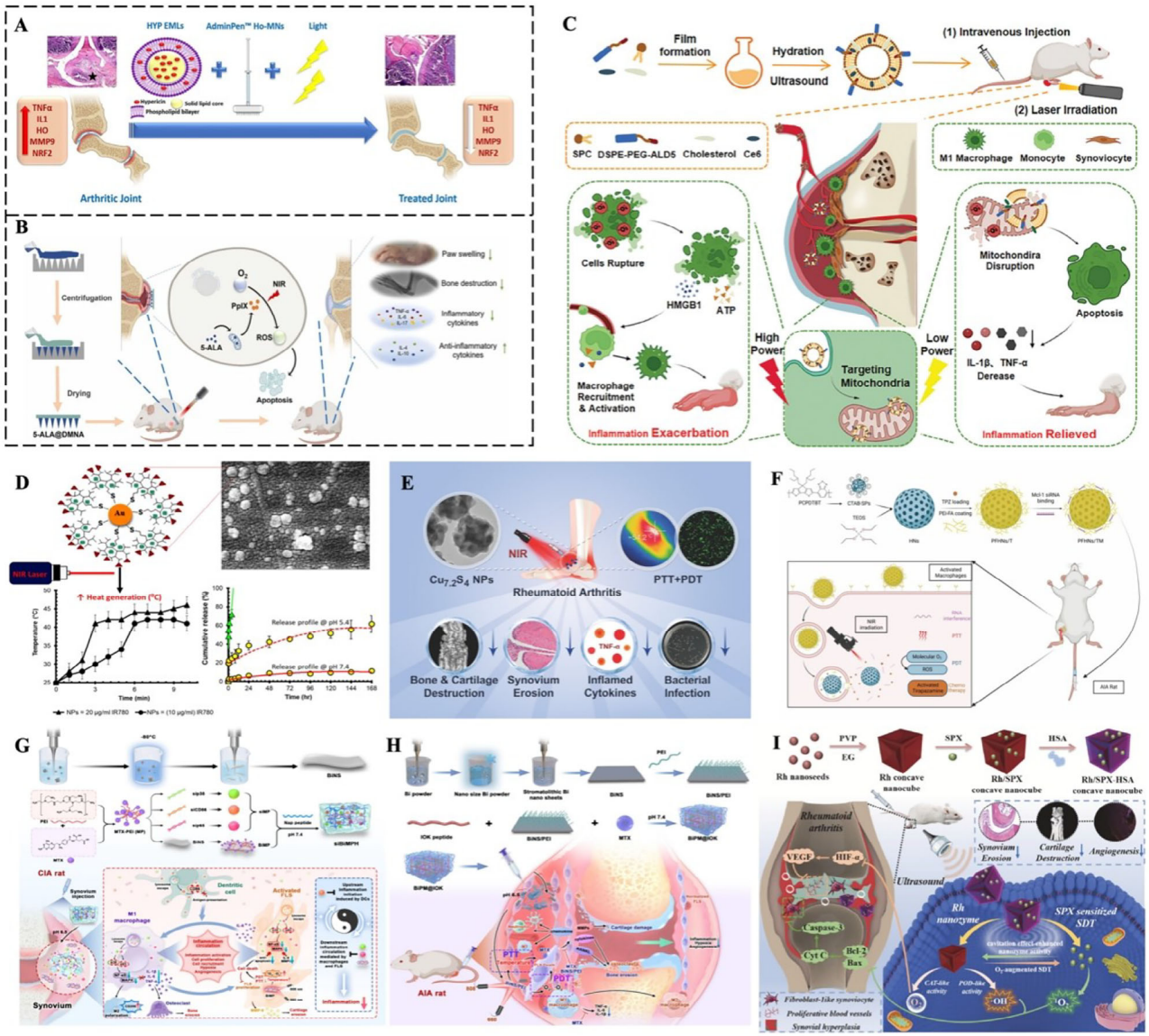

Figure 9. PDT/SDT combined strategies for bone degenerative disorders. A) HYP-EMLs/Ho-MNs synergistic strategy for targeted RA immune modulation. Reproduced with permission.[127] Copyright 2024, Elsevier. B) 5-ALA@DMNA microneedles: synthesis route and dual-action therapeutic mechanism. Reproduced with permission.[128] Copyright 2023, Elsevier. C) Mitochondrial-targeted "less-is-more" PDT: Ce6@M-Lip. Reproduced with permission.[130] Copyright 2015, Springer Nature. D) Au-DEN-MTX-IR780 multimodal nanoplatform for NIR-II photothermal/chemodynamic synergy. Reproduced with permission.[132] Copyright 2019, Elsevier. (E) $Cu_{7.2}S_4$ nanozyme-driven tri-modal therapy. Reproduced with permission.[134] Copyright 2018, Wiley-VCH. F) PFHNs/TM nanohybrid: synthesis mechanism and in vivo inflammation resolution/bone remodeling axis. Reproduced with permission.[140] Copyright 2022, Taylor & Francis. G) siBiMPNH nanotherapeutic system. Reproduced with permission.[141] Copyright 2024, Elsevier. H) BiPM@IOK dual-function nanoregulator: macrophage polarization control + hyperplastic synoviocyte depletion in refractory RA. Reproduced with permission.[142] Copyright 2024, Springer Nature. I) Rh-SPX/HSA nanocomplex. Reproduced with permission.[149] Copyright 2021, Elsevier.

(**Figure 9A**). The HYP-EMLs, prepared through thin-film hydration, demonstrated superior transdermal penetration (1560 μm depth in human skin) compared to free HYP. This nanocarrier-based delivery system establishes a targeted therapeutic platform for localized RA intervention.

Porphyrin-Based PS for RA-PDT: Development of Multifunctional Theranostic Strategies: Porphyrin-based compounds show established efficacy for RA therapy. A dissolvable microneedle array encapsulating 5-aminolevulinic acid (5-ALA@DMNA) enabled spatially controlled PDT[128] (Figure 9B). Following intracellular conversion to PpIX within RA-FLS, 635 nm irradiation (100 mW cm^{-2}) triggered ROS generation, which suppressed cell migration and induced apoptosis via ROS-dependent mechanisms. Complementarily, verteporfin (BPD-MA) achieved optimal therapeutic outcomes at 2 mg kg^{-1}.[129] Recent advances include theranostic composites like TSPP-TiO_2 nanocrystal hybrids (TP) for early inflammation detection and precision therapy[130] (Figure 9C). Upon 635 nm activation, TP gen-

erated cytotoxic ROS and $^1O_2$, selectively promoting RA-FLS apoptosis and reducing serum IL-17/TNF-α, with fluorescence imaging confirming TP accumulation at pre-symptomatic joints 16 days before clinical manifestation. Post-treatment outcomes demonstrated expanded joint spacing, reduced synovial erosion, decreased leukocyte/lymphocyte infiltration, and absent hemotoxicity.

Dye-Based PS for RA-PDT: Low-Power PDT and Multimodal Synergistic Therapy: To resolve the conflicting efficacy-safety profile of PDT in RA (low-power PDT insufficiently eliminating pro-inflammatory cells versus high-power PDT exacerbating inflammation), Zou et al.[131] engineered mitochondrial-targeted liposomes (Ce6@M-Lip) modified with ApoPep-5 peptide (Figure 9C). This strategy achieved efficient Ce6 accumulation in the mitochondria of pro-inflammatory macrophages, enhancing low-power PDT efficacy while preventing HMGB1 release-triggered persistent inflammation under high-power conditions. Concurrently, Pandey[132] designed IR780-gold nanohybrid dendrimers (Au-DEN-MTX-IR780 NPs) for RA chemo-photothermal-photodynamic triple therapy (Figure 9D). Gold nanoparticles were functionalized with thiolated dendrimers (DEN), covalently linked to MTX, and loaded with the NIR photosensitizer IR780. NPs targeted inflammatory joints via MTX, where IR780 generated photothermal effects under 808-nm laser irradiation and synergized with MTX to amplify ROS production.

Capitalizing on fibroblast activation protein (FAP) overexpression in RA cells, Dorst et al.[133] designed anti-FAP antibody-IRDye7000DX conjugates for selective ablation of FAP^+ synovial fibroblasts. FAP-targeted PDT (FAP-tPDT) demonstrated high specificity and biosafety, though further optimization of illumination protocols and repeat dosing is required to sustain therapeutic effects.

Metal-Organic Framework PS: Suppression of RA-FLS Proliferation and Hypoxia Mitigation: Numerous metal-based PS architectures have been explored. Lu et al.[134] synthesized cysteine-modified flower-like $Cu_{7.2}S_4$ nanoparticles via a one-pot method, pioneering their application in RA PDT-PTT combination therapy (Figure 9E). NIR-activated $Cu_{7.2}S_4$ preserved bone architecture with increased bone mineral density (BMD) and bone volume/total volume ratios, while suppressing synovial hyperplasia, cartilage erosion, and pro-inflammatory cytokine expression.

Building on copper-based materials, Huang[135] designed yolk-shell octahedral Au NR@CuS nanoparticles for multimodal RA treatment. By integrating Au nanorod (NR) plasmonic effects with CuS-derived photothermal/catalytic properties, they achieved 67.2% photothermal conversion efficiency and generated hydroxyl radicals (·OH) via Fenton-like reactions and photocatalysis. Hyaluronic acid (HA) and vasoactive intestinal peptide (VIP) modifications enabled synovium targeting, while MTX loading provided chemotherapeutic synergy. This platform exemplifies precision-targeted multimodality for RA.

MOF-based nanosystems have recently demonstrated therapeutic potential in RA. Zhao et al.[136] and Zhang et al.[137] independently developed HA-modified MOF platforms targeting CD44-overexpressing macrophages. Zhao's FT-HA-MTX NPs utilized Fe^{3+} to catalyze ·OH/O_2 generation from H_2O_2, alleviating hypoxia-mediated PDT resistance while combining photothermal/PDT effects. Zhang's TPNPs-HA employed PCN-224 for 660 nm-triggered ROS production and hypoxia-activated tirapazamine (TPZ) release. Both systems showed excellent biocompatibility, offering multi-mechanistic synergism for precise RA treatment.

Bio-Derived and Hydrogel-Based Photosensitizing Nanoplatforms: Integrated Polytherapeutic Theranostics: Emerging PSs are increasingly explored for RA-PDT. Gabriel et al.[138] developed a thrombin-sensitive prodrug (T-PS) by conjugating pheophorbide a to a PEGylated polylysine carrier via a thrombin-cleavable peptide linkage. Thrombin-mediated cleavage restored PS fluorescence and phototoxicity. T-PS combined with 665 nm photoirradiation (25 J cm^{-2}) significantly induced synovial apoptosis. This thrombin-activated strategy presents a low-toxicity therapeutic approach; however, longitudinal studies are required to evaluate its sustained efficacy and capacity to mitigate inflammation-driven sequelae.

Li's team pioneered multimodal RA nanotherapies.[139] Folate-targeted mesoporous silica nanoparticles (SMPFs) co-encapsulated a semiconducting polymer (PCPDTBT) and hypoxia-activated tirapazamine (TPZ). NIR irradiation triggered chemo-photothermal-photodynamic synergy, reducing macrophage viability and alleviating rat adjuvant-induced arthritis (AIA). Subsequently, folate-PEI-coated hollow nanoparticles (PFHNs/TM, Figure 9F) co-delivered TPZ and Mcl-1 siRNA,[140] silencing the antiapoptotic protein to synergize with PTT, PDT, and hypoxia-activated chemo (HaCT)—establishing a quadruple mechanism (QTM). Both systems demonstrated folate-targeted delivery and biocompatibility but need optimization of phototherapeutic penetration and siRNA lysosomal escape for clinical translation.

Recent innovations integrate stimuli-responsive hydrogels for multitarget RA therapy. Wu et al.[141] developed pH-sensitive nap-peptide hydrogels (siBiMPNH) encapsulating CD86/NF-κB/MAPK-p38 siRNA and bismuthene nanosheets (BiNS), releasing payloads in acidic synovial microenvironments (Figure 9G). siRNA suppressed dendritic cell/macrophage activity while BiNS-mediated PTT/PDT (808/660 nm) eradicated FLS. Parallelly, they engineered IOK peptide hydrogels (BiPM@IOK) co-loading MTX and BiNS/PEI[142] (Figure 9H) for pH-triggered release. MTX inhibited macrophage activation, and BiNS phototherapy eliminated FLS, synergistically promoting cartilage repair—exemplifying novel immune-microenvironment modulation strategies. These platforms exemplify novel immunomodulation-microenvironment remodeling strategies for RA.

5.1.2. Osteoarthritis Pathogenesis

OA causes damage to nearly all joint components and is accompanied by varying degrees of localized functional impairment. Traditional surgical or chemotherapeutic interventions face challenges such as perioperative management burdens, adverse drug reactions, and poor targeting. PDT, a promising non-invasive modality, demonstrates significant potential in OA management by spatially confining oxidative damage to pathological cells while sparing adjacent healthy tissues.

Currently, research on PDT for OA remains limited,[143] with a predominant focus on the photosensitizer Ce6. Zharova demonstrated preferential accumulation of Ce6 in inflamed synovium of OA-affected knees.[144] Upon irradiation with a 662 nm laser (120–150 J cm^{-2}), Ce6 induced apoptosis and markedly ameliorated synovitis. Furthermore, the team elucidated that Ce6 reduced caspase-3 levels in OA synovium to confer anti-inflammatory effects and identified 3.2 mg kg^{-1} as the optimal therapeutic dose.[145] Notably, while they verified the short-term safety of PDT, comprehensive evaluations of Ce6-PDT's chronic toxicity remain unaddressed.

5.2. SDT in Degenerative Bone Disorders: Mechanical Stress Control and Oxidative Balance

SDT has limited applications in degenerative and metabolic bone diseases, with only sparse reports on its successful use in RA.

Wu et al.[146] engineered ferroferric oxide nanoparticles (Fe_3O_4 NPs) loaded with PpIX into live macrophages, termed Fe_3O_4-PpIX@Mφs, which homed to inflamed joints via cytokine-guided migration. The Fe_3O_4 NP incorporation enhanced PpIX payload capacity and accelerated US-triggered drug release. Meanwhile, PpIX-mediated SDT synergized with Fe^{3+}-driven Fenton reactions (generating hydroxyl radicals ·OH) to exert anti-inflammatory effects. Their strategy effectively eradicated inflammatory cells in RA, proposing a novel targeted therapeutic approach.

Tang et al. validated the efficacy of the sonosensitizer ICG in RA-SDT.[147] They innovatively developed oxygen and ICG-loaded PLGA nanoparticles (OI-NPs) to enhance sonophotodynamic therapy (SPDT) targeting against RA fibroblast-like synoviocytes (MH7A).[148] Following dual 808 nm laser (0.75 W cm^{-2}) and focused ultrasound (1.0 W cm^{-2}) irradiation, OI-NPs elevated ROS production by 1.4-fold compared to free ICG. This nanosystem alleviated hypoxic microenvironments via oxygen release triggered by phase transition, offering a novel RA treatment strategy. However, strategies for clinical translation require prioritized attention.

Additionally, the sonosensitizer sparfloxacin (SPX) has been explored for RA therapy. Li et al. designed concave cubic rhodium-based nanozymes (Rh/SPX-HSA) co-loaded with SPX and human serum albumin (HSA) to overcome the limitations of synovial hypoxia on RA-SDT efficacy.[149] As illustrated in Figure 9I, these nanozymes simultaneously exhibit peroxidase (POD)- and catalase (CAT)-like activities, catalytically decomposing synovial H_2O_2 into ·OH and O_2. This dual enzymatic action alleviates local hypoxia and amplifies SPX-mediated $^1O_2$ generation.

6. Bone Regeneration

6.1. PDT in Bone Regeneration: Anti-Infective Osseointegration and Stem Cell Activation

Traumatic heterotopic ossification (HO), triggered by aberrant differentiation of mesenchymal stromal cells into chondrogenic and osteogenic tissues, faces clinical challenges such as high recurrence rates and side effects with current therapies (surgical resection, radiotherapy). Zheng Wang et al.[150] targeted the early chondrogenic phase of HO and proposed a PDT-based strategy using a NIR probe, WL-808, composed of a collagen type II-targeting peptide (WYRGRL) conjugated with the photosensitizer IR-808. Under 808 nm laser irradiation, WL-808 generates ROS to induce chondrocyte apoptosis and suppress ossification (**Figure 10A**). However, the ROS production efficiency of WL-808 was reduced compared to IR-808 alone, necessitating further optimization of this nanocomposite design.

Several nanoparticles (NPs) exhibit dual functionality in suppressing biofilm formation on bone implants while enhancing osteogenesis. For instance, Huang et al. developed a titanium-based implant material, Ti-RP-IR780-RGDC, integrating anti-infective and osseointegration properties.[151] Fabricated via hydrothermal and coating techniques, this material leverages the photothermal conversion capability of red phosphorus (RP) for mild PTT. Combined with IR780-mediated ROS generation under 808 nm laser (PDT), it synergistically disrupts biofilms. The RGDC peptide further facilitates osteogenic differentiation.

S.Y. Wu et al.[152] developed NIR-responsive titanate/TiO_2–X coatings (KMNW/NaMNS) on titanium implants via one-step hydrothermal synthesis (Figure 10B). Mimicking bone ECM, the hierarchical coating eradicated biofilms and enhanced osteoblast adhesion via micro/nanotopography, upregulating osteogenic genes (ALP, Runx2, OCN). This study offers a novel surface modification strategy for titanium implants with dual anti-infective and osseointegrative capabilities. In a parallel approach, Yuan et al. developed Ti-M/I/RGD (as described earlier),[106] which combines ICG to achieve anti-infective and osteogenic functions. Additionally, BPD-MA irradiated with a 690 nm laser has been reported to ablate tumors while suppressing osteoclast-mediated bone resorption, thereby promoting tumor-associated bone defect repair.[153]

Diabetes significantly exacerbates bone disease severity. Managing its severe complications and diabetes-orthopedic comorbidities presents a major clinical challenge. Studies show PDT effectively prevents diabetic foot amputations.[154] Ren et al.[155] developed a multifunctional nanosystem, HMSN-GOX-LArg@Ce6IL, to address key diabetic foot ulcer (DFU) challenges: drug-resistant biofilm infection, local hyperglycemia, and impaired circulation. This system comprises hollow mesoporous silica nanoparticles (HMSNs) co-loaded with glucose oxidase (GOX) and L-arginine (LArg), immobilized with Ce6IL. It combats biofilm infection while moderately promoting wound healing. Although exhibiting some hemolysis (<5%), it demonstrated acceptable biocompatibility without significant systemic toxicity, offering a novel clinical strategy for diabetes-bone comorbidities. Additionally, TBO-chit-Au-AgNPs (Akhtar et al.) effectively control DFU progression, markedly accelerating lesion healing alongside biofilm elimination.[156]

6.2. SDT in Bone Regeneration: Acoustic-Stimulated Mineralization and Repair Acceleration

SDT is currently predominantly utilized to expedite bone regeneration in infectious bone defects. Based on Ti_3C_2 nanosheets,

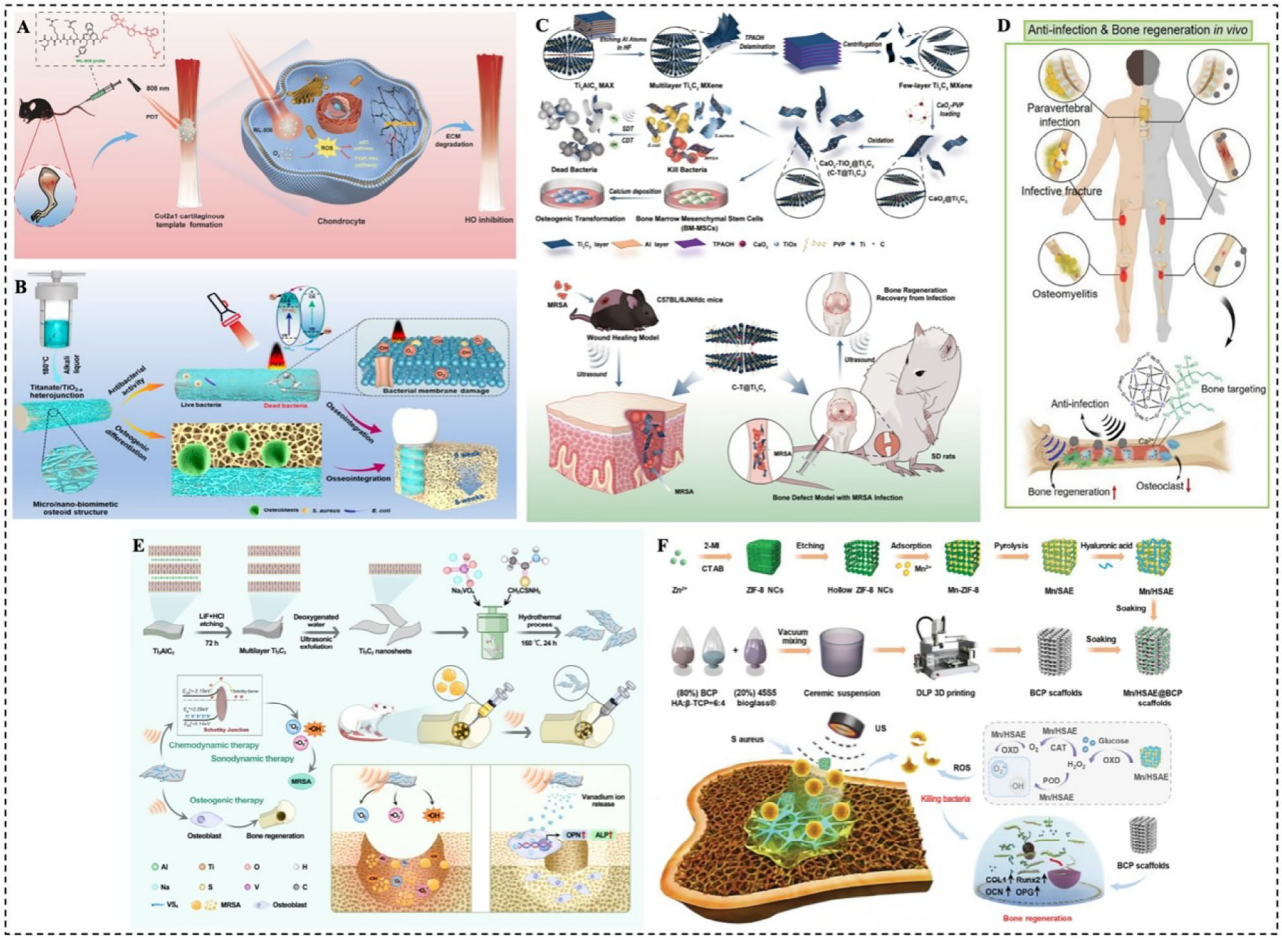

Figure 10. PDT/SDT promotes bone regeneration through multi-pathway activation. A) Composition and mechanism of WL-808. Reproduced with permission.[150] Copyright 2023, Elsevier. B) Fabrication of biomimetic Ti-titanate/TiO_2–X heterostructures for implant-associated infection treatment and osseointegration. Reproduced with permission.[152] Copyright 2024, American Chemical Society (ACS). C) Synthesis and dual-mode application of C-T@Ti_3C_2 nanosheets. Reproduced with permission.[157] Copyright 2023, Springer Nature. D) In vivo targeted repair of infectious bone tissues via HN25. Reproduced with permission.[158] Copyright 2023, Wiley-VCH. E) 3VSM-based therapy for infectious bone defects. Reproduced with permission.[159] Copyright 2024, Springer Nature. F) Mn/HSAE@BCP synthesis and functional mechanism. Reproduced with permission.[160] Copyright 2024, Wiley-VCH.

Wang et al. previously developed HN-Ti_3C_2 using a HNTM strategy (as described in detail earlier).[19] Meanwhile, Yu et al.[157] engineered CaO_2-TiOx@Ti_3C_2 nanosheets via Ti_3C_2 MXene oxidation by CaO_2, generating Ti^{3+}/Ti^{4+}-containing TiOx. In acidic microenvironments, H_2O_2 release triggers ·OH generation via Fenton reaction (CDT), while ultrasound activates TiOx for ROS production (Figure 10C). This nanocatalytic platform addresses deep orthopedic infections synergistically.

In a related approach, Ma et al.[158] synthesized ALN-modified defect-engineered porphyrinic metal-organic frameworks (HN25), which effectively eradicated MRSA infections while enhancing bone repair through dual mechanisms: suppression of osteoclast activity and modulation of the redox microenvironment (Figure 10D). Additionally, an ultrasound-responsive VS_4/MXene Schottky heterojunction nanomaterial (VSM) was reported for synergistic treatment of MRSA-infected bone defects.[159] Synthesized via a hydrothermal method, VSM comprises VS_4 nanorods anchored on two-dimensional Ti_3C_2 MXene substrates. This heterojunction system integrates robust antibacterial effects (via CDT/SDT synergy) with osteogenic capacity, offering a non-invasive strategy for managing infected bone defects (Figure 10E).

Furthermore, Gao et al.[160] designed a 3D-printed biphasic calcium phosphate (BCP) scaffold functionalized with manganese single-atom nanozymes (Mn/HSAE@BCP). The scaffold catalyzes H_2O_2 conversion into ROS within acidic microenvironments. Under SDT, it generated substantial ROS, exhibiting potent antibacterial activity against *S. aureus* and *E. coli* while enhancing osteogenic markers (COL1, Runx2, OCN, OPG) to accelerate bone regeneration in infected defects (Figure 10F).

7. Conclusions and Future Perspectives

This review summarizes recent advances in the application of PDT and SDT for bone-related pathologies. Although PDT and SDT have been explored in various contexts and shown promis-

ing outcomes, most studies remain confined to the design, development, and preclinical validation of photo-/sonosensitizers in animal models. Translating these findings into clinical practice represents a significant undertaking and continues to face numerous shared challenges.

7.1. Current Clinical Challenges

(1) Tissue Penetration and Energy Delivery Efficiency: In photodynamic therapy (PDT), visible light (<700 nm wavelength) exhibits limited penetration depth (<5 mm), which hinders the effective treatment of deep-seated bone tumors or infected lesions. While SDT offers superior tissue penetration capacity, the uneven energy distribution of acoustic fields may compromise treatment precision. (2) Biosafety and Pharmacokinetics of Sensitizers: Current photosensitizers and sonosensitizers, such as porphyrin derivatives and ICG, face critical clinical translation barriers due to inherent limitations. Poor aqueous solubility in agents like mTHPC and zinc phthalocyanine compromises formulation stability and bioavailability. Rapid systemic clearance, exemplified by ICG's hepatic elimination within minutes, hinders therapeutic accumulation in bone. Furthermore, potential phototoxicity—manifested by prolonged cutaneous photosensitivity following BPD-MA administration—necessitates post-treatment light avoidance; long-term retention risks, including splenic and hepatic sequestration of porphyrins, require chronic toxicity monitoring. Critically, comprehensive assessments remain underdeveloped: detailed in vivo degradation profiles are lacking for chlorin e6, and longitudinal studies evaluating chronic outcomes like nephrotoxicity from metal-based NPs (e.g., TiO_2) are insufficient.To bridge this safety-efficacy gap, advanced material design must integrate toxicological profiling with therapeutic optimization. Rigorous assessment of organ-specific toxicity, dose-dependent risks, and immunogenicity should align with efficacy metrics to define viable therapeutic indices. Ignoring these priorities undermines translational validity, as seen in repeated failures to achieve sustained tumor control without off-target damage in complex bone microenvironments. (3) Complex Modulation of Tumor Microenvironments: Hypoxic zones in bone tumors significantly impair PDT efficacy, while ROS-scavenging proteins (e.g., MTH1) and immunosuppressive microenvironments further restrict therapeutic outcomes. Additionally, biofilm formation in infectious bone diseases reduces antibacterial PDT/SDT susceptibility. (4) Insufficient Standardization of Treatment Parameters: Optimization of light/sound intensity, frequency, and sensitizer dosage lacks standardized protocols. Moreover, translational mechanisms bridging preclinical studies and clinical demands remain underexplored, limiting the reproducibility and safety of therapeutic regimens. (5) Mechanistic Complexity in Multimodal Synergistic Therapies: Combining PDT/SDT with chemotherapy, immunotherapy, or gene therapy holds potential, but their synergistic mechanisms—such as temporal sequence effects and dose dependency—require in-depth elucidation to mitigate risks of off-target effects or hyperactivated immune responses.

With shifting patterns of global diseases, comorbidity rates involving other conditions such as diabetes and skeletal disorders are gradually but steadily increasing.[161] How PDT/SDT addresses these comorbidity challenges has emerged as a critical research topic.

7.2. Emerging Therapeutic Opportunities

1) Development of Novel Sensitizers: Designing multifunctional nanosensitizers (e.g., MXene-based heterojunctions, metal single-atom catalysts) with near-infrared-II (NIR-II) responsiveness, hypoxia-activated or oxygen self-supplying capabilities, coupled with targeting modifications (e.g., bone-homing peptides, antibody conjugation) to enhance lesion-specific accumulation efficiency.
2) Construction of PSDT Combined Therapy Systems: Integrating the spatiotemporal synergy of PDT and SDT (PSDT), leveraging sonodynamic effects to enhance photosensitizer penetration or utilizing photothermal effects to promote acoustic cavitation, thereby achieving dual-targeting eradication of deep-seated lesions.
3) Microenvironment Modulation and Immune Reprogramming: Developing ROS-responsive nanocarriers combined with immune checkpoint inhibitors (e.g., anti-PD-1) or ferroptosis inducers to reverse tumor-immunosuppressive microenvironments.[162] Additionally, catalytically decomposing H_2O_2 or neutralizing acidic microenvironments may alleviate oxygen-dependent limitations of PDT/SDT.
4) Intelligent Theranostic Platforms: Advanced platforms integrating diagnostic imaging modalities (e.g., NIR-II fluorescence, photoacoustic imaging) with PDT/SDT therapeutic functions will enable precise spatiotemporal control. These systems leverage artificial intelligence algorithms to dynamically optimize light/sound parameters based on real-time feedback, ensuring accurate dosimetry delivery tailored to heterogeneous tissue environments. It is also possible to leverage AI technology to identify appropriate sensitizers and aid in the development of intricate multifunctional nanoparticles.[163] IoT-enabled sensors facilitate real-time treatment response monitoring by tracking physiological biomarkers (e.g., tissue oxygenation, ROS generation) and structural changes in bone lesions. Coupled with predictive analytics, this integrated approach supports data-driven personalization of therapeutic protocols to maximize efficacy while minimizing off-target effects in complex orthopedic microenvironments.
5) Clinical Translation and Standardization: Establishing patient stratification-based treatment guidelines and conducting multicenter clinical trials to validate long-term safety. Promoting Good Manufacturing Practice (GMP)-compliant large-scale production of nanosensitizers and refining regulatory frameworks to accelerate their translation from bench to bedside.

Through interdisciplinary innovation and technological convergence, PDT/SDT holds promise in overcoming current therapeutic limitations, offering efficient and personalized non-invasive solutions for bone-related pathologies (**Figure 11**).

7.3. Concluding Remarks

PDT and SDT, as non-invasive precision therapeutic modalities, demonstrate unique potential for managing bone-related

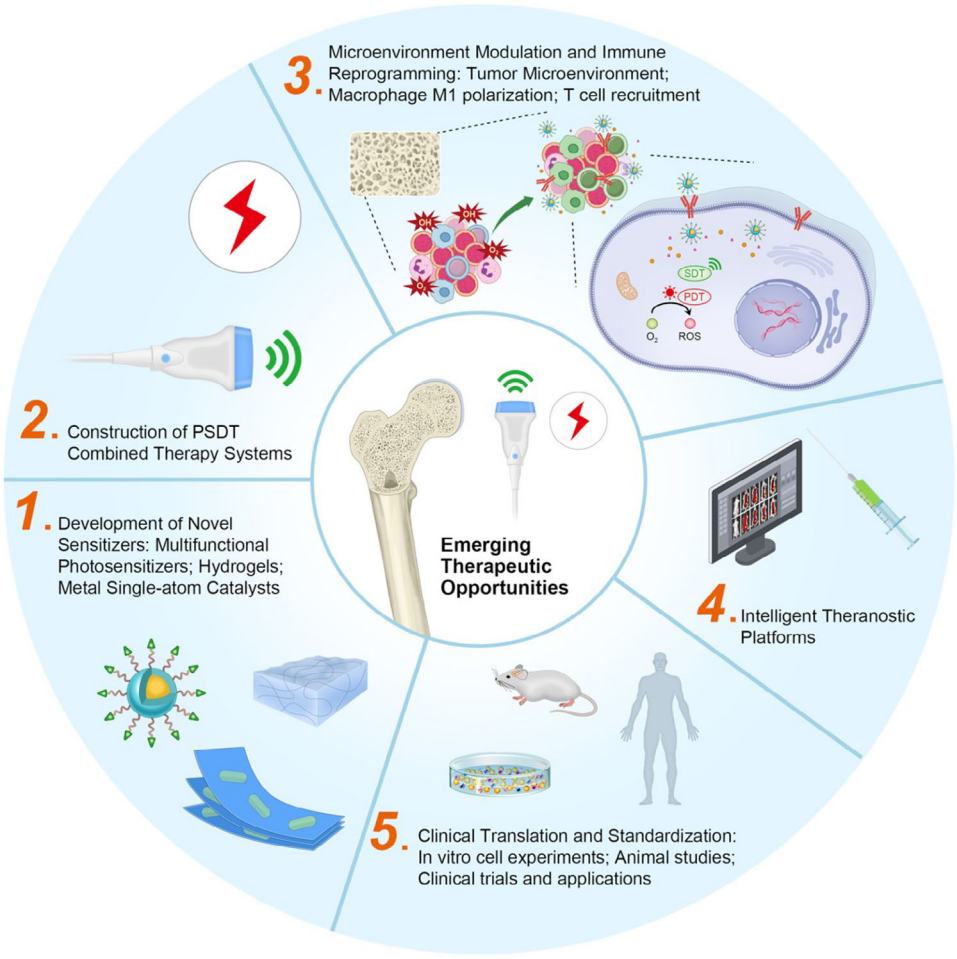

Figure 11. Perspectives on PDT and SDT in orthopedic applications.

pathologies. PDT enables targeted ablation of pathological cells via type I (free radical cascade) and type II (singlet oxygen) reactions mediated by photosensitizers, and has been successfully applied in preclinical studies of superficial bone tumors and infectious bone defects. In contrast, SDT leverages the deep-tissue penetration of ultrasound waves combined with mechanochemical damage induced by acoustic cavitation, offering non-invasive intervention strategies for deep-seated lesions such as osteomyelitis and bone metastases. However, their clinical translation remains limited by the unique pathological features of bone diseases: energy attenuation caused by the highly mineralized bone matrix, hypoxia and immunosuppression in tumor microenvironments that impair ROS generation efficiency, and heterogenous bone anatomical structures hindering targeted sensitizer delivery.

To address these challenges, multi-mechanistic synergistic strategies represent critical avenues to overcome current therapeutic limitations. Recent studies indicate that combining PDT/SDT with immune checkpoint inhibitors activates antitumor immune responses by inducing ICD, thereby reversing immunosuppressive microenvironments. Smart carriers loaded with catalytic nanomaterials (e.g., CeO_2@MXene, metal single-atom enzymes) can catalyze endogenous H_2O_2 decomposition to generate oxygen, alleviating hypoxia-induced restrictions on ROS production. Bio-inspired targeting systems (e.g., bone-homing peptide-functionalized or cell membrane-camouflaged nanoparticles) significantly enhance sensitizer accumulation efficiency in complex bone microenvironments. Furthermore, the photosonodynamic collaborative therapy (PSDT) achieves spatiotemporal energy complementarity, enabling simultaneous precision ablation of superficial lesions and deep-tissue penetration, providing innovative solutions for multifocal bone diseases.

Despite promising preclinical validation of PDT/SDT efficacy, clinical translation faces multiple obstacles: insufficient long-term biocompatibility and pharmacokinetic data for photosensitizers/sonosensitizers; lack of standardized protocols for treatment parameters (e.g., light dose, acoustic intensity, and irradiation sequence); and mechanistic complexity and potential off-target risks in multimodal combined therapies. These factors impede the initiation of large-scale clinical trials and reproducibility of therapeutic outcomes.

Future research should prioritize three domains: novel sensitizer development, integration of intelligent theranostic technologies, and translational medical validation. Through multidimensional advancements in material innovation, technical convergence, and clinical verification, PDT/SDT could overcome lim-

itations of conventional therapies, establishing a transformative paradigm for bone disease management that ultimately improves patient prognosis and quality of life.

Acknowledgements

P.W. and W.X. contributed equally to this work. This work was supported by the National Key R&D Program of China (2023YFC3603400), National Natural Science Foundation of China (82472522, 92268115), Projects of International Cooperation and Exchanges NSFC (W2421123), Hunan Provincial Science Fund for Distinguished Young Scholars (2024JJ2089), Horizontal Research Funding of Central South University (JXDY-ZD-20231101), and the Independent Exploration and Innovation Project for Postgraduate Students of Central South University (2024ZZTS0163).

Conflict of Interest

The authors declare no conflict of interest.

Keywords

musculoskeletal disorders, photodynamic therapy, photosensitizer, sonodynamic therapy, sonosensitizer

Received: May 21, 2025
Revised: June 30, 2025
Published online:

[1] L. M. Gehrig, *Am. J. Surg.* **2011**, *202*, 364.
[2] S. Safiri, A.-A. Kolahi, M. Cross, C. Hill, E. Smith, K. Carson-Chahhoud, M. A. Mansournia, A. Almasi-Hashiani, A. Ashrafi-Asgarabad, J. Kaufman, M. Sepidarkish, S. K. Shakouri, D. Hoy, A. D. Woolf, L. March, G. Collins, R. Buchbinder, *Arthritis Rheumatol.* **2021**, *73*, 702.
[3] Z. Zhang, R. Wang, H. Xue, S. Knoedler, Y. Geng, Y. Liao, M. Alfertshofer, A. C. Panayi, J. Ming, B. Mi, G. Liu, *Biomater. Res.* **2023**, *27*, 123.
[4] Z. Wan, P. Zhang, L. Lv, Y. Zhou, *Theranostics* **2020**, *10*, 11837.
[5] L. Nistor, *J. Bone Jt. Surg., Am. Vol.* **1981**, *63*, 394.
[6] J. Liao, R. Han, Y. Wu, Z. Qian, *Bone Res.* **2021**, *9*, 18.
[7] G. Tan, J. Xu, Q. Yu, Z. Yang, H. Zhang, *Photodiagn. Photodyn. Ther.* **2022**, *40*, 103093.
[8] Y. Hou, D. i. Zhao, X. Yang, C. Guo, M. Wen, J. Bao, G. Qu, H. Meng, *Oncol. Rep.* **2023**, *50*, 198.
[9] M. D. Daniell, J. S. Hill, *Aust. N. Z. J. Surg.* **1991**, *61*, 340.
[10] T. J. Dougherty, G. Lawrence, J. H. Kaufman, D. Boyle, K. R. Weishaupt, A. Goldfarb, *J. Natl. Cancer Inst.* **1979**, *62*, 231.
[11] Q. Ren, C. Yi, J. Pan, X. Sun, X. Huang, *Int. J. Nanomed.* **2022**, *17*, 3385.
[12] J. Wang, S. Liang, S. Chen, T. Ma, M. Chen, C. Niu, Y. i. Leng, L. Wang, *J. Nanobiotechnol.* **2024**, *22*, 328.
[13] R. R. Allison, K. Moghissi, *Clin. Endosc.* **2013**, *46*, 24.
[14] Z. Meng, H. Xue, T. Wang, B. Chen, X. Dong, L. Yang, J. Dai, X. Lou, F. Xia, *J. Nanobiotechnol.* **2022**, *20*, 344.
[15] C. A. Robertson, D. H. Evans, H. Abrahamse, *J. Photochem. Photobiol., B* **2009**, *96*, 1.
[16] S. Kwiatkowski, B. Knap, D. Przystupski, J. Saczko, E. Kedzierska, K. Knap-Czop, J. Kotlinska, O. Michel, K. Kotowski, J. Kulbacka, *Biomed. Pharmacother.* **2018**, *106*, 1098.
[17] Z. Luksiene, *Medicina (Kaunas)* **2003**, *39*, 1137.
[18] K. Plaetzer, B. Krammer, J. Berlanda, F. Berr, T. Kiesslich, *Lasers Med. Sci.* **2009**, *24*, 259.
[19] H. Wang, N. a. Mu, Y. He, X. Zhang, J. Lei, C. Yang, L. Ma, Y. Gao, *Theranostics* **2023**, *13*, 1669.
[20] G. Canavese, A. Ancona, L. Racca, M. Canta, B. Dumontel, F. Barbaresco, T. Limongi, V. Cauda, *Chem. Eng. J.* **2018**, *340*, 155.
[21] G.-Y. Wan, Y. Liu, B. o.-W. Chen, Y.-Y. Liu, Y.-S. Wang, N. Zhang, G.-Y. Wan, Y. Liu, B.-W. Chen, Y.-Y. Liu, Y.-S. Wang, N. Zhang, *Cancer Biol. Med.* **2016**, *13*, 325.
[22] S. Son, J. H. Kim, X. Wang, C. Zhang, S. A. Yoon, J. Shin, A. Sharma, M. H. Lee, L. Cheng, J. Wu, J. S. Kim, *Chem. Soc. Rev.* **2020**, *49*, 3244.
[23] Y. Zhang, Q. Zhang, F. Wang, M. Li, X. Shi, J. Li, *Nano Lett.* **2023**, *23*, 7699.
[24] R. Shao, Y. Wang, L. Li, Y. Dong, J. Zhao, W. Liang, *Drug Delivery* **2022**, *29*, 1631.
[25] G. W. Siegel, J. S. Biermann, A. A. Calinescu, D. E. Spratt, N. J. Szerlip, *Curr. Osteoporos. Rep.* **2018**, *16*, 512.
[26] B. White, V. Rossi, P. J. Baugher, *Photomed. Laser Surg.* **2016**, *34*, 400.
[27] R. Adachi, T. Nakamura, K. Nakata, T. Uchiyama, T. Hagi, K. Asanuma, A. Sudo, *Anticancer Res.* **2024**, *44*, 963.
[28] S. M. Sachsenmaier, F. Traub, A. Cykowska, et al., *Biology (Basel)* **2021**, *10*, 1070.
[29] I. Coupienne, G. Fettweis, J. Piette, *Lasers Surg. Med.* **2011**, *43*, 557.
[30] H. Chen, D. Zheng, W. Pan, X. Li, B. Lv, W. Gu, J. O.'. Machuki, J. Chen, W. Liang, K. Qin, J. Greven, F. Hildebrand, Z. Yu, X. Zhang, K. Guo, *ACS Appl. Mater. Interfaces* **2021**, *13*, 19710.
[31] G. N. Makhadmeh, A. Abdul Aziz, *Artif. Cells, Nanomed., Biotechnol.* **2018**, *46*, 1043.
[32] H. Zeng, M. Sun, C. Zhou, F. Yin, Z. Wang, Y. Hua, Z. Cai, *PLoS One* **2013**, *8*, 77727.
[33] V. H. Fingar, P. K. Kik, P. S. Haydon, P. B. Cerrito, M. Tseng, E. Abang, T. J. Wieman, *Br. J. Cancer* **1999**, *79*, 1702.
[34] J. Z. Yao, W. N. Zhang, C. Q. Sheng, Z. Y. Miao, F. Yang, J. X. Yu, L. Zhang, Y. L. Song, T. Zhou, Y. J. Zhou, *Bioorg. Med. Chem. Lett.* **2008**, *18*, 293.
[35] M. Sun, C. Zhou, H. Zeng, F. Yin, Z. Wang, J. Yao, Y. Hua, Z. Cai, *J. Photochem. Photobiol., B* **2016**, *160*, 178.
[36] H.-Y. Gong, M.-X. Sun, S. Hu, Y.-Y. Tao, B. o. Gao, G.-D. Li, Z.-D. Cai, J.-Z. Yao, *Asian Pac. J. Cancer Prev.* **2013**, *14*, 3351.
[37] S. Duchi, G. Sotgiu, E. Lucarelli, M. Ballestri, B. Dozza, S. Santi, A. Guerrini, P. Dambruoso, S. Giannini, D. Donati, C. Ferroni, G. Varchi, *J. Controlled Release* **2013**, *168*, 225.
[38] Y. Ding, W. Yu, R. Shen, X. Zheng, H. Zheng, Y. Yao, Y. Zhang, C. Du, H. Yi, *Adv. Healthcare Mater.* **2024**, *13*, 2303308.
[39] K. Reidy, C. Campanile, R. Muff, W. Born, B. Fuchs, *Photochem. Photobiol.* **2012**, *88*, 721.
[40] D. Meier, S. M. Botter, C. Campanile, B. Robl, S. Gräfe, G. Pellegrini, W. Born, B. Fuchs, *Int. J. Cancer* **2017**, *140*, 1680.
[41] J. Xiao, H. Xiao, Y. Cai, J. Liao, J. Liu, L. Yao, S. Li, *Oncol. Res.* **2024**, *32*, 691.
[42] Y. Gao, Z. Wang, X. Jin, X. Wang, Y. Tao, S. Huang, Y. Wang, Y. Hua, X. Guo, J. Xu, Z. Cai, *Adv. Healthcare Mater.* **2024**, *13*, 2400538.
[43] W. Li, Y. Yang, J. Wang, T. Ge, S. Wan, L. Gui, Y. Tao, P. Song, L. Yang, F. Ge, W. Zhang, *J. Mech. Behav. Biomed. Mater.* **2024**, *150*, 106306.
[44] W. Liu, J. Zhang, L. Ding, W. Ni, J. Yuan, H. Xiao, J. Zhang, *Biomater. Sci.* **2021**, *9*, 7228.
[45] Q. Song, W. Yang, X. Deng, Y. Zhang, J. Li, X. Xing, W. Chen, W. Liu, H. Hu, Y. Zhang, *Colloids Surf., B* **2022**, *218*, 112715.
[46] X. Deng, R. Zhao, Q. Song, Y. Zhang, H. Zhao, H. Hu, Z. Zhang, W. Liu, W. Lin, G. Wang, *Drug Delivery* **2022**, *29*, 3142.
[47] Q. Zuo, Y. Ou, S. Zhong, H. Yu, F. Zhan, M. Zhang, *Acta Biochim. Biophys. Sin. (Shanghai)* **2021**, *53*, 1387.

[48] S. Zhong, Y. Zhang, H. Mou, et al., *Aging (Albany NY)* **2024**, *16*, 2789.
[49] F. Zhan, T. He, Z. Chen, Q. Zuo, Y. Wang, Q. Li, S. Zhong, Y. Ou, *Cell Biosci.* **2021**, *11*, 179.
[50] F. Zhan, Y. e. Zhang, Q. Zuo, C. Xie, H. Li, L. Tian, C. Wu, Z. Chen, C. Yang, Y. Wang, Q. Li, T. He, H. Yu, J. Chen, J. Xiang, Y. Ou, *Photodiagnosis Photodyn. Ther.* **2022**, *39*, 102964.
[51] H. Yu, Y. e. Zhang, Q. Zuo, S. Zhong, Y. Chen, M. Zhang, F. Zhan, Y. Ou, *Photodiagnosis Photodyn. Ther.* **2022**, *37*, 102646.
[52] Q. Huang, Y. S. Ou, Y. Tao, H. Yin, P. H. Tu, *Apoptosis* **2016**, *21*, 749.
[53] Y. Chen, H. Yin, Y. Tao, S. Zhong, H. Yu, J. Li, Z. Bai, Y. Ou, *Int. J. Mol. Med.* **2020**, *45*, 971.
[54] K. Kusuzaki, H. Murata, T. Matsubara, H. Satonaka, T. Wakabayashi, A. Matsumine, A. Uchida, *In Vivo* **2007**, *21*, 205.
[55] C. Fotia, S. Avnet, K. Kusuzaki, L. Roncuzzi, N. Baldini, *Curr. Pharm. Des.* **2015**, *21*, 4088.
[56] S. A. Elfeky, A. Elsayed, M. Moawad, W. A. Ahmed, *Photodiagnosis Photodyn. Ther.* **2020**, *32*, 102056.
[57] S.-L. Lu, Y.-H. Wang, G.-F. Liu, L. Wang, Y. Li, Z.-Y. Guo, C. Cheng, *Front. Mol. Biosci.* **2021**, *8*, 663089.
[58] W.-N. Zeng, Q.-P. Yu, D. Wang, J.-L. i. Liu, Q.-J. Yang, Z.-K. e. Zhou, Y. i.-P. Zeng, *J. Nanobiotechnol.* **2021**, *19*, 79.
[59] Z. Jiang, Y. Pan, J. Wang, J. Li, H. Yang, Q. Guo, S. Liang, S. Chen, Y. Hu, L. Wang, *Biomater. Sci.* **2022**, *10*, 2345.
[60] S. Lenna, C. Bellotti, S. Duchi, E. Martella, M. Columbaro, B. Dozza, M. Ballestri, A. Guerrini, G. Sotgiu, T. Frisoni, L. Cevolani, G. Varchi, M. Ferrari, D. M. Donati, E. Lucarelli, *J. Exp. Clin. Cancer Res.* **2020**, *39*, 40.
[61] W. Yu, M. Ye, J. Zhu, Y. Wang, C. Liang, J. Tang, H. Tao, Y. Shen, *Nanomedicine* **2018**, *14*, 1099.
[62] W. Yu, Y. Wang, J. Zhu, L. Jin, B. Liu, K. Xia, J. Wang, J. Gao, C. Liang, H. Tao, *Biomaterials* **2019**, *192*, 128.
[63] Y.-X. Ge, H.-J. Zhuang, T.-W. Zhang, H.-F. Liang, W. Ding, L. Zhou, Z.-R. Dong, Z.-C. Hu, Q. Chen, J. Dong, L.-B. Jiang, X.-F. Yin, *Mater. Today Bio* **2023**, *19*, 100547.
[64] F. Zhang, J. Chen, W. Luo, C. Wen, W. Mao, Y. Yang, C. Liu, Y. Xu, W. Chen, L. Wen, *Int. J. Pharm.* **2024**, *652*, 123865.
[65] Y. Wang, L. Zhang, G. Zhao, Y. Zhang, F. Zhan, Z. Chen, T. He, Y. Cao, L. Hao, Z. Wang, Z. Quan, Y. Ou, *J. Nanobiotechnol.* **2022**, *20*, 83.
[66] D. Ziental, B. Czarczynska-Goslinska, D. T. Mlynarczyk, A. Glowacka-Sobotta, B. Stanisz, T. Goslinski, L. Sobotta, *Nanomaterials* **2020**, *10*, 387.
[67] Y. Liang, C. Liao, X. Guo, G. Li, X. Yang, J. Yu, J. Zhong, Y. Xie, L. Zheng, J. Zhao, *Small* **2023**, *19*, 2205511.
[68] M. Zorrón, A. L. Cabrera, R. Sharma, J. Radhakrishnan, S. Abbaszadeh, M. A. Shahbazi, O. A. Tafreshi, S. Karamikamkar, H. Maleki, *Adv. Sci. (Weinheim, Ger.)* **2024**, *11*, 2403204.
[69] B. Zheng, R. Zhang, F. Kuang, T. Hui, C. Fu, L. Zhang, C. Zhou, M. Qiu, B. Yue, *J. Mater. Chem. B* **2024**, *12*, 1816.
[70] W. Gu, Z. Hua, Z. Li, Z. Cai, W. Wang, K. Guo, F. Yuan, F. Gao, H. Chen, *Biomater. Sci.* **2021**, *10*, 216.
[71] J. Cheng, W. Wang, X. Xu, Z. Lin, C. Xie, Y. Zhang, T. Zhang, L. Li, Y. Lu, Q. i. Li, *Mater. Sci. Eng., C* **2020**, *107*, 110324.
[72] J. Y. Zhang, S. Chen, P. Wang, D. J. Jiang, D. X. Ban, N. Z. Zhong, G. C. Jiang, H. Li, Z. Hu, J. R. Xiao, Z. G. Zhang, W. W. Cao, *Nanoscale* **2017**, *9*, 2706.
[73] Y. Yuan, S. Diao, X. Ni, D. Zhang, W. Yi, C. Jian, X. Hu, D. Li, A. Yu, W. Zhou, Q. Fan, *J. Nanobiotechnol.* **2022**, *20*, 44.
[74] Y. Yu, D. Tang, C. Liu, Q. i. Zhang, L. Tang, Y. Lu, H. Xiao, *Adv. Mater.* **2022**, *34*, 2105976.
[75] J. Wan, X. Zhang, D. Tang, T. Liu, H. Xiao, *Adv. Mater.* **2023**, *35*, 2209799.
[76] X. An, D. Zhong, W. Wu, R. Wang, L. Yang, Q. Jiang, M. Zhou, X. Xu, *ACS Appl. Mater. Interfaces* **2024**, *16*, 6868.
[77] P. Tu, Q. Huang, Y. Ou, X. Du, K. Li, Y. Tao, H. Yin, *Oncol. Rep.* **2016**, *35*, 3209.
[78] K.-T. Li, Q. Chen, D.-W. Wang, Q.-Q. Duan, S. i. Tian, J.-W. He, Y.-S. Ou, D.-Q. Bai, *Cancer Med.* **2016**, *5*, 3186.
[79] G. N. Makhadmeh, A. Abuelsamen, M. H. Al-Akhras, A. A. Aziz, *Photodiagnosis Photodyn. Ther.* **2022**, *38*, 102801.
[80] W. Tang, Q. Liu, X. Wang, P. Wang, J. Zhang, B. Cao, *Ultrasonics* **2009**, *49*, 786.
[81] W. Tang, Q. Liu, X. Wang, P. Wang, B. Cao, N. Mi, J. Zhang, *J. Ultrasound Med.* **2008**, *27*, 645.
[82] W. Tang, Q. Liu, J. Zhang, B. Cao, P. Zhao, X. Qin, *Ultrasonics* **2010**, *50*, 567.
[83] X. Liu, W. Li, S. Geng, Q. G. Meng, Z. G. Bi, *Mol. Med. Rep.* **2015**, *12*, 1183.
[84] Q. Liu, X. Wang, P. Wang, L. Xiao, Q. Hao, *Cancer Chemother. Pharmacol.* **2007**, *60*, 671.
[85] X. B. Wang, Q. H. Liu, P. Wang, K. Zhang, W. Tang, B. L. Wang, *Cancer Biother. Radiopharm.* **2008**, *23*, 238.
[86] P. Wang, X. Wang, K. Zhang, K. Gao, M. Song, Q. Liu, *Ultrasonics* **2013**, *53*, 935.
[87] Y. Li, Q. i. Zhou, Z. Hu, B. Yang, Q. Li, J. Wang, J. Zheng, W. Cao, *PLoS One* **2015**, *10*, 0132074.
[88] C. Li, K. Zhang, P. Wang, J. Hu, Q. Liu, X. Wang, *Biopharm. Drug Dispos.* **2014**, *35*, 50.
[89] W. Xiong, P. Wang, J. Hu, Y. Jia, L. Wu, X. Chen, Q. Liu, X. Wang, *Sci. Rep.* **2015**, *5*, 17485.
[90] N. Nomikou, C. Sterrett, C. Arthur, B. McCaughan, J. F. Callan, A. P. McHale, *ChemMedChem* **2012**, *7*, 1465.
[91] C. Komori, K. Okada, K. Kawamura, S. Chida, T. Suzuki, *Anticancer Res.* **2009**, *29*, 2411.
[92] M. Gong, Y. Huang, H. Feng, J. Lin, A. Huang, J. Hu, Q. Tang, X. Zhu, S. Han, J. Lu, J. Wang, *J. Controlled Release* **2023**, *355*, 68.
[93] C. Zhou, X. Xie, H. Yang, S. Zhang, Y. Li, C. Kuang, S. Fu, L. Cui, M. Liang, C. Gao, Y. Yang, C. Gao, C. Yang, *Mol. Pharm.* **2019**, *16*, 2956.
[94] I. Zlotver, A. Sosnik, *Small* **2024**, *20*, 2305475.
[95] B. Geng, X. Yang, P. Li, W. Shi, D. Pan, L. Shen, *ACS Appl. Mater. Interfaces* **2021**, *13*, 45325.
[96] N. Sun, Q. Lei, M. Wu, S. Gao, Z. Yang, X. Lv, R. Wei, F. Yan, L. Cai, *Mater. Today Bio* **2024**, *26*, 101053.
[97] Y. Zhang, Y. Wang, A. Zhu, N. Yu, J. Xia, J. Li, *Angew. Chem., Int. Ed. Engl.* **2024**, *63*, 202310252.
[98] N. Yumita, Y. Iwase, S. I. Umemura, F. S. Chen, Y. Momose, *Anticancer Res.* **2020**, *40*, 2549.
[99] S. K. Bisland, S. Burch, *Photodiagnosis Photodyn. Ther.* **2006**, *3*, 147.
[100] S. K. Bisland, C. Chien, B. C. Wilson, S. Burch, *Photochem. Photobiol. Sci.* **2006**, *5*, 31.
[101] C. L. Pan, M. H. Chen, F. I. Tung, T. Y. Liu, *Acta Biomater.* **2017**, *47*, 159.
[102] X. Yin, Z. Fang, Y. Fang, L. Zhu, J. Pang, T. Liu, Z. Zhao, J. Zhao, *Front. Microbiol.* **2022**, *13*, 876166.
[103] J. A. Reis Jr., F. B. de Carvalho, R. F. Trindade, P. N. de Assis, P. F. de Almeida, A. L. Pinheiro, *Lasers Med. Sci.* **2014**, *29*, 789.
[104] J. A. dos Reis, J. N. dos Santos, B. S. Barreto, P. N. de Assis, P. F. Almeida, A. L. B. Pinheiro, *J. Photochem. Photobiol., B* **2015**, *149*, 235.
[105] X. Lu, R. Chen, J. Lv, W. Xu, H. Chen, Z. Ma, S. Huang, S. Li, H. Liu, J. Hu, L. Nie, *Acta Biomater.* **2019**, *99*, 363.
[106] Z. Yuan, B. Tao, Y. He, C. Mu, G. Liu, J. Zhang, Q. Liao, P. Liu, K. Cai, *Biomaterials* **2019**, *223*, 119479.
[107] F. Jiang, J. Wang, Z. Ren, Y. Hu, B. Wang, M. Li, J. Yu, J. Tang, G. Guo, Y. Cheng, P. Han, H. Shen, *ACS Nano* **2024**, *18*, 6990.
[108] X. Xie, J. Wei, B. Zhang, W. Xiong, Z. He, Y. Zhang, C. Gao, Y. Zhao, B. o. Liu, *J. Nanobiotechnol.* **2022**, *20*, 416.

[109] W.-S. Kuo, C.-Y. Chang, J.-C. Liu, J.-H. Chen, E. C. So, P.-C. Wu, *Int. J. Nanomed.* **2020**, *15*, 6813.
[110] C. Chao, L. Kang, W. Dai, C. Zhao, J. Shi, B. Tong, Z. Cai, Y. Dong, *J. Mater. Chem. B* **2023**, *11*, 3106.
[111] H. Tang, X. Qu, W. Zhang, X. Chen, S. Zhang, Y. Xu, H. Yang, Y. Wang, J. Yang, W.-E. n. Yuan, B. Yue, *Adv. Mater.* **2022**, *34*, 2107300.
[112] Y. Qiao, X. Liu, Y. Zheng, Y. u. Zhang, Z. Li, S. Zhu, H. Jiang, Z. Cui, S. Wu, *ACS Nano* **2024**, *18*, 17086.
[113] W. Wang, X. Cheng, J. Liao, Z. Lin, L. Chen, D. Liu, T. Zhang, L. Li, Y. Lu, H. Xia, *ACS Biomater. Sci. Eng.* **2019**, *5*, 6243.
[114] H. Lin, C. Yang, Y. Luo, M. Ge, H. Shen, X. Zhang, J. Shi, *ACS Nano* **2022**, *16*, 5943.
[115] X. Feng, J. Lei, L. Ma, Q. Ouyang, Y. Zeng, H. Liang, C. Lei, G. Li, L. Tan, X. Liu, C. Yang, *Small* **2022**, *18*, 2105775.
[116] S. Chen, J. Wang, K. Tang, H. Liao, Y. Xu, L. Wang, C. Niu, *Int. J. Nanomed.* **2022**, *17*, 4525.
[117] X. Yang, R. Fang, X. Li, W. Kong, Y. Jin, R. Jiao, Z. Liu, M. Zhang, Q. Peng, Y. Zhang, N. Song, *ACS Appl. Mater. Interfaces* **2025**, *17*, 11795.
[118] Q. Zheng, X. Liu, S. Gao, Z. Cui, S. Wu, Y. Liang, Z. Li, Y. Zheng, S. Zhu, H. Jiang, R. Zou, *Small* **2023**, *19*, 2207687.
[119] Y. Zeng, Q. Ouyang, Y. i. Yu, L. Tan, X. Liu, Y. Zheng, S. Wu, *Small Methods* **2023**, *7*, 2201248.
[120] X. Feng, L. Ma, J. Lei, Q. Ouyang, Y. Zeng, Y. Luo, X. Zhang, Y. u. Song, G. Li, L. Tan, X. Liu, C. Yang, *ACS Nano* **2022**, *16*, 2546.
[121] Y. i. Yu, L. Tan, Z. Li, X. Liu, Y. Zheng, X. Feng, Y. Liang, Z. Cui, S. Zhu, S. Wu, *ACS Nano* **2021**, *15*, 10628.
[122] F. Lu, X. Wu, H. Hu, Z. He, J. Sun, J. Zhang, X. Song, X. Jin, G. Chen, *Microbiol. Spectrum* **2022**, *10*, 0054422.
[123] Z. Li, Y. Lu, J. Song, P. Han, H. Shi, X. Yao, X. Zhang, G. Zhang, *J. Colloid Interface Sci.* **2025**, *684*, 122.
[124] Y. Cheng, Y. Zhang, Z. Zhao, G. Li, J. Li, A. Li, Y. Xue, B. Zhu, Z. Wu, X. Zhang, *Adv. Mater.* **2022**, *34*, 2206646.
[125] H. Abd-El-Azim, I. A. Tekko, A. Ali, A. Ramadan, N. Nafee, N. Khalafallah, T. Rahman, W. Mcdaid, R. G. Aly, L. K. Vora, S. J. Bell, F. Furlong, H. O. McCarthy, R. F. Donnelly, *J. Controlled Release* **2022**, *348*, 849.
[126] K. Zhang, S. Gao, J. Guo, G. Ni, Z. Chen, F. Li, X. Zhu, Y. Wen, Y. Guo, *Iran. J. Basic Med. Sci.* **2018**, *21*, 130.
[127] H. Abd-El-Azim, H. Abbas, N. El Sayed, M. R. Mousa, H. M. Elbardisy, M. Zewail, *Int. J. Pharm.* **2024**, *653*, 123876.
[128] Y. Li, L. Zheng, W. Cao, X. Yang, Q. Wang, X. Gu, F. Liu, T. Ma, X. u. Wang, Q. Wang, *Biomed. Pharmacother.* **2023**, *162*, 114684.
[129] C. Hendrich, G. Hüttmann, J. L. Vispo-Seara, S. Houserek, W. E. Siebert, *Knee Surg. Sports Traumatol. Arthrosc.* **2000**, *8*, 190.
[130] C. Zhao, F. Ur Rehman, Y. Yang, X. Li, D. Zhang, H. Jiang, M. Selke, X. Wang, C. Liu, *Sci. Rep.* **2015**, *5*, 11518.
[131] Q. Zuo, J. Lyu, X. Shen, F. Wang, L. Xing, M. Zhou, Z. Zhou, L. Li, Y. Huang, *Small* **2024**, *20*, 2307261.
[132] P. K. Pandey, R. Maheshwari, N. Raval, P. Gondaliya, K. Kalia, R. K. Tekade, *J. Colloid Interface Sci.* **2019**, *544*, 61.
[133] D. N. Dorst, M. Rijpkema, M. Boss, B. Walgreen, M. M. A. Helsen, D. L. Bos, M. Brom, C. Klein, P. Laverman, P. M. van der Kraan, M. Gotthardt, M. I. Koenders, M. Buitinga, *Rheumatology (Oxford)* **2020**, *59*, 3952.
[134] Y. Lu, L. Li, Z. Lin, L. Wang, L. Lin, M. Li, Y. Zhang, Q. Yin, Q. Li, H. Xia, *Adv. Healthcare Mater.* **2018**, *7*, 1800013.
[135] R. Huang, C. Zhang, Y. Bu, Z. Li, X. Zheng, S. Qiu, J. O.'. Machuki, L. Zhang, Y. Yang, K. Guo, F. Gao, *Biomaterials* **2021**, *277*, 121088.
[136] H. Zhao, J. Wei, Y. He, Y. Wu, L. Ge, C. Zheng, *Colloids Surf., B* **2024**, *239*, 113952.
[137] S. Zhang, M. Zhang, J. Zhang, G. e. Li, X. Lu, F. Sun, W. Liu, *Colloids Surf., B* **2024**, *234*, 113707.
[138] D. Gabriel, N. Lange, V. Chobaz-Peclat, M. F. Zuluaga, R. Gurny, H. van den Bergh, N. Busso, *J. Controlled Release* **2012**, *163*, 178.
[139] X. Li, S. Zhang, X. Zhang, Y. Hou, X. Meng, G. e. Li, F. Xu, L. Teng, Y. Qi, F. Sun, Y. Li, *Int. J. Pharm.* **2021**, *607*, 120947.
[140] X. Li, S. Zhang, M. Zhang, G. e. Li, B. o. Yang, X. Lu, L. Teng, Y. Li, F. Sun, *Int. J. Nanomed.* **2022**, *17*, 6257.
[141] Y. Wu, Z. Wang, Y. Ge, Y. Zhu, T. Tian, J. Wei, Y. Jin, Y. i. Zhao, Q. Jia, J. Wu, L. Ge, *J. Controlled Release* **2024**, *370*, 747.
[142] Y. Wu, Y. Ge, Z. Wang, Y. Zhu, T. Tian, J. Wei, Y. Jin, Y. i. Zhao, Q. Jia, J. Wu, L. Ge, *J. Nanobiotechnol.* **2024**, *22*, 188.
[143] M. i. Zhang, W. Hu, C. Cai, Y. Wu, J. Li, S. Dong, *Mater. Today Bio* **2022**, *14*, 100223.
[144] T. A. Zharova, S. V. Ivannikov, A. M. Tonenkov, E. P. h. Stranadko, L. A. Semenova, M. M. Smorchkov, V. I. Makarov, I. D. Romanishkin, A. V. Ryabova, V. B. Loschenov, *Photodiagnosis Photodyn. Ther.* **2016**, *15*, 88.
[145] T. A. Zharova, E. A. Kogan, V. I. Makarov, M. M. Smorchkov, A. V. Lychagin, S. V. Ivannikov, N. V. Zharkov, V. B. Loschenov, *Photodiagnosis Photodyn. Ther.* **2020**, *30*, 101669.
[146] L. Wu, K. Zhao, L. Xu, J. Cui, L. i. Ruan, S. Bei, J. Cao, X. Qi, S. Shen, *Ultrason. Sonochem.* **2024**, *107*, 106928.
[147] Q. Tang, S. Chang, Z. Tian, J. Sun, L. Hao, Z. Wang, S. Zhu, *Ultrasound Med. Biol.* **2017**, *43*, 2690.
[148] Q. Tang, J. Cui, Z. Tian, J. Sun, Z. Wang, S. Chang, S. Zhu, *Int. J. Nanomed.* **2017**, *12*, 381.
[149] W. Li, Y. Song, X. Liang, Y. Zhou, M. Xu, Q. Lu, X. Wang, N. Li, *Biomaterials* **2021**, *276*, 121063.
[150] Z. Wang, C. Sun, Y. Yu, D. Zhang, B. Qi, Z. Li, X. Yi, A. Yu, *Mater. Today Bio* **2023**, *23*, 100822.
[151] B. Huang, L. Tan, X. Liu, J. Li, S. Wu, *Bioact. Mater.* **2019**, *4*, 17.
[152] S. Wu, Q. Zhang, D. Lin, B. A. Al-Shaaobi, Y. Sun, W. Si, X. Ding, P. Ma, X. Shen, J. Liu, *ACS Appl. Mater. Interfaces* **2024**, *16*, 43227.
[153] L. Wise-Milestone, M. K. Akens, V. C. K. Lo, A. J. Yee, B. C. Wilson, C. M. Whyne, *Breast Cancer Res. Treat.* **2012**, *133*, 899.
[154] J. P. Tardivo, F. Adami, J. A. Correa, M. A. Pinhal, M. S. Baptista, *Photodiagn. Photodyn. Ther.* **2014**, *11*, 342.
[155] J. Ren, C. Wang, H. Gao, S. Lu, C. Fu, H. Wang, G. Wang, Z. Zhu, H. Wu, W. Luo, Y. Zhang, *Adv. Healthcare Mater.* **2025**, *14*, 2403282.
[156] F. Akhtar, A. U. Khan, B. Qazi, S. Kulanthaivel, P. Mishra, K. Akhtar, A. Ali, *Sci. Rep.* **2021**, *11*, 24464.
[157] Y. Yu, H. Sun, Q. Lu, J. Sun, P. Zhang, L. Zeng, K. Vasilev, Y. Zhao, Y. Chen, P. Liu, *J. Nanobiotechnol.* **2023**, *21*, 193.
[158] L. Ma, Y. Cheng, X. Feng, X. Zhang, J. Lei, H. Wang, Y. Xu, B. Tong, D. Zhu, D. Wu, X. Zhou, H. Liang, K. Zhao, K. Wang, L. Tan, Y. Zhao, C. Yang, *Adv. Mater.* **2024**, *36*, 2307846.
[159] Y. He, X. Liu, J. Lei, L. Ma, X. Zhang, H. Wang, C. Lei, X. Feng, C. Yang, Y. Gao, *J. Nanobiotechnol.* **2024**, *22*, 31.
[160] Z. Gao, Z. Song, R. Guo, M. Zhang, J. Wu, M. Pan, Q. Du, Y. He, X. Wang, L. Gao, Y. Jin, Z. Jing, J. Zheng, *Adv. Healthcare Mater.* **2024**, *13*, 2303182.
[161] C. J. L. Murray, *Lancet* **2024**, *403*, 2259.
[162] T. Luo, Z. Fan, A. Zeng, A. Wang, Y. Pan, Y. Xu, H. Chen, W. Chen, D. Nie, J. Lin, A. Huang, M. Gong, Y. Huang, Y. Ding, X. Zhu, L. Rao, J. Wang, *Adv. Sci. (Weinheim, Ger.)* **2025**, *12*, 2410427.
[163] W.-H. Yin, Y. Liu, H.-H. Huang, P.-Y. Li, X. Liu, F.-Q. Bai, *J. Org. Chem.* **2025**, *90*, 1825.

Zhong Da received his Doctor of Surgery degree from Xiangya Hospital, Central South University, in 2008. He is currently a Chief Physician/Professor and Doctoral Supervisor at Xiangya Hospital, Central South University, and also serves as the Director of the Digital Orthopedics Center at the same institution. His primary clinical and research interests include hip- and knee-joint preservation, joint replacement and revision, and digital orthopaedic technologies.

Zhou Li received his Bachelor's degree from Wuhan University in 2004 and his Doctor's degree from Peking University in 2010. From 2015 to 2025 he served as Doctoral Supervisor and Deputy Director at the Institute of Nanoenergy and Nanosystems, Chinese Academy of Sciences (CAS), and as Professor at the University of the Chinese Academy of Sciences. Since 2025 he has been Professor at Tsinghua Changgung Hospital, School of Clinical Medicine, Tsinghua University, and Professor at the School of Biomedical Engineering, Tsinghua University. He was honored with the National Natural Science Fund for Distinguished Young Scholars in 2021 and has also received the Beijing Natural Science Fund for Distinguished Young Scholars, among other notable awards. His research focuses on the advancement of bioelectronic and medical devices, namely in the areas of wearable and implantable electronic health monitoring and therapy devices, biosensors, biodegradable electronics, and biomechanical investigations.

Yusheng Li received his M.D and Ph.D. degree from Central south university in 2011, specializing in Orthopedics. From 2016–2019, he worked as a postdoctoral fellow at the department of Orthopedic surgery, Johns Hopkins university. He currently is an associate professor and associate chief physician at the department of Orthopedics, Xiangya hospital, Central South university. His research focuses on Orthopedic degenerative diseases and sports injury.